33RD CONGRESS
OF THE INTERNATIONAL COUNCIL
OF THE AERONAUTICAL SCIENCES
STOCKHOLM, SWEDEN, 4-9 SEPTEMBER, 2022

ICAS 2022 SWEDEN

# RECENT ACTIVITIES ON FLOW QUALITY ASSESSMENT AT THE EUROPEAN TRANSONIC WINDTUNNEL

Dr. Jae Hun You[1], Martin C.N. Wright[1] & Dr. Harald Quix[1]

[1]European Transonic Windtunnel GmbH, Cologne, Germany

## Abstract

The European Transonic Windtunnel (ETW) is a worldwide unique aerodynamic testing facility enabling investigations of laminar flow at high real-flight Reynolds and Mach numbers. With the increasing interest in laminar flow testing, and around 25 years after the primary flow quality assessment and several changes to the tunnel circuit, ETW was approached to reassess its test-section flow characteristics. Therefore, ETW recently performed extensive unsteady flow-quality assessment campaigns over a wide range of ETW's operating Mach and Reynolds numbers. The aim of this task was acquiring for the empty test section a comprehensive flow-quality reference dataset including spectral characteristics thereby supporting future laminar flow tests at ETW. The new flow quality assessment employed a rotating survey rake and a three-arm checkout probe to obtain flow quantities in ETW's empty test section. Flow characteristics of ETW's two standard high-speed test section configurations, the full-span and half-sapn model slotted wall configurations, respectively, were assessed. In addition, the effects of ETW's different Mach number control methods on the test-section flow quality were intensively investigated. The present paper gives a detailed overview of the employed instrumentation components and their calibration as well as a comprehensive summary of the test program. The paper also summarises results from the primary analysis. These first results already show ETW's outstanding ability to perform high-Reynolds-number laminar flow testing at low subsonic conditions as well as transonic Mach numbers.

**Keywords:** cryogenic wind tunnel, flow quality assessment, high Reynolds-number testing

## 1. Introduction

The European Transonic Windtunnel (ETW) is an advanced aerodynamic testing facility for simulating aerodynamic performance of scaled aircraft up to real-flight Reynolds and Mach numbers. Its unique capability to simulate efficiently high Reynolds numbers and the ability to separate Reynolds number, Mach number and model deformation effects make ETW an indispensable tool for aircraft manufacturers to validate and optimise their designs already at an early stage of aircraft development process. Particularly due to its high Reynolds number capability and high flow quality, ETW is to date the only option to both industry and academia for laminar flow investigations at real-flight Reynolds and Mach numbers. Indeed, with increasing interest in laminar flow applications on various aircraft components to improve the aerodynamic efficiency and thereby to lower CO2 emissions, laminar flow testing with the application of temperature sensitive paint (TSP) technique to locate the laminar-turbulent boundary layer transition became one of ETW's core business activities in the last decade. Extensive investigation on ETW's flow quality during its calibration phase in the mid-90s confirmed the ETW's high flow quality relating to turbulence intensity and the outstanding uniformity of Mach number as well as the temperature distribution across the test section [1, 2]. The possibility of laminar flow testing at ETW was evaluated in the European research project TELFONA in the mid-00s by comparing measured Tollmien-Schlichting and crossflow dominated transition locations with computed ones using the $e^N$ Method [3]. Since that time, however, some modifications of the tunnel circuit

were implemented in order to further enhance the ETW's flow characteristics and performance capability as well as operating efficiency. For instance, a tail cone was attached to the downstream support (see Fig. 1) of the compressor to avoid flow unsteadiness caused by possible vortex formation, and a new wall slot configuration was introduced to extend ETW's capability to half-span model testing [4]. Therefore, ETW recently performed several flow-quality assessment (FQA) campaigns to answer demands for the reassessment of test-section flow characteristics around 25 years after the initial flow quality assessment. The new flow quality assessment was conducted within the framework of the German research project LuFo-LoCaRe (Lokalisierung und Charakterisierung von flugrelevanten Lärmquellen an Hochauftriebssystemen).
The objective of recent activities was to acquire in the empty test section a comprehensive flow-quality reference dataset over an extensive range of ETW's operating Reynolds and Mach numbers and for different test section wall configurations as well as for different testing procedures and thereby supporting data analysis of future laminar flow testing at ETW. This dataset shall include measured spectral characteristics of the flow, which are on the one hand cleaned from sensor setup related artifacts e.g. hot-wire prong or rake vibrations and on the other hand are relevant in terms of the transitional boundary layer receptivity, buffet or aeroelastic phenomena (focus to 10 Hz - 30,000 Hz). In the following sections, a detailed description of the new flow quality assessment, including a comprehensive summary of the test program and an overview of the employed instrumentation components as well as their calibration, is given. The paper also summarises the primary results that already confirm ETW's outstanding ability to perform high-Reynolds-number laminar flow testing at low subsonic conditions as well as transonic Mach numbers.

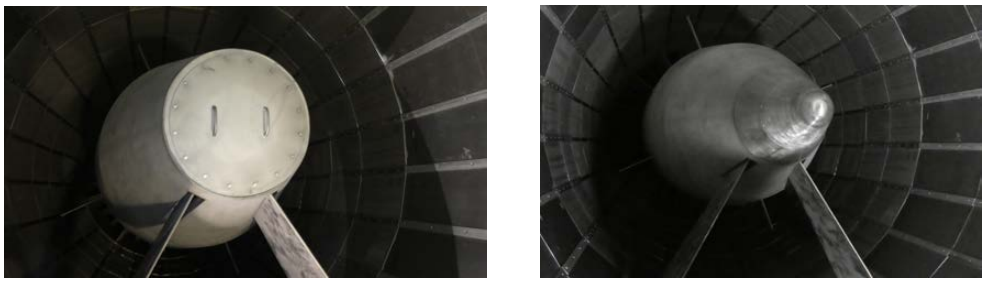

(a) Before modification (b) After modification

Figure 1 – Modification of downstream support of compressor.

## 2. Facility Description

ETW (see Fig. 2) is a cryogenic, pressurised, transonic wind tunnel for real-flight Reynolds number testing, operated by three European countries, Germany, the United Kingdom and the Netherlands. The operating Mach number range extends from the low speed conditions at $M = 0.13$, through the relevant transonic regime for transport aircraft, to the low supersonic speeds up to $M = 1.35$. The facility uses pure nitrogen of high quality as the working medium in order to achieve the test temperature range from 313 K down to 110 K and operating pressure levels from 110 kPa up to 450 kPa. The combined effects of low temperatures and moderately high pressure enable a maximum chord Reynolds number of 50 million and 90 million, for full-span models (span about 1.6 m) and half-span models (semi-span about 1.3 m), respectively, at representative cruise Mach numbers for modern transport aircraft. Fig. 3 shows ETW's performance envelope expressed as a function of Reynolds and Mach numbers.
In contrast to conventional wind tunnels, ETW can vary flow velocity, temperature and pressure independently. This unique capability allows the opportunity for individual investigations of the following effects:

- Reynolds number effects – Reynolds number is varied by changing only the flow temperature, while keeping the Mach number and total pressure, and thus the dynamic pressure, constant. As a result, a pure viscous effect can be investigated without varying the aeroelastic distortion of the model.

Figure 2 – ETW aerial view.

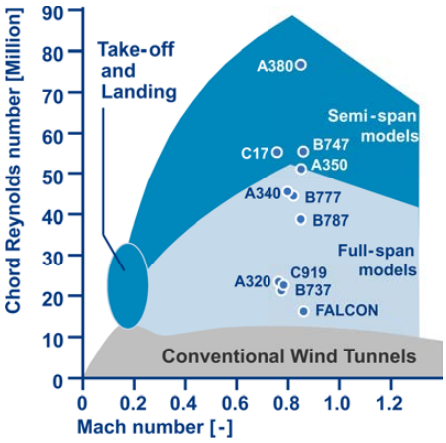


Figure 3 – ETW performance envelope.

- Mach number effects – investigation of pure compressibility effects is possible without varying the dynamic pressure and Reynolds number. It is achieved by a simultaneous change of the total pressure and temperature.
- Dynamic pressure effects – aeroelastic model-deformation effects can be studied by varying the dynamic pressure, while keeping the Mach number and Reynolds number constant.

ETW has a closed, continuous-flow aerodynamic circuit with the test section height of 2 m, width of 2.4 m and length of 9 m (see Fig. 4). In order to reduce interferences between the lifting surfaces of model and the test section walls, slots may be opened. Therefore, the top and bottom wall slots (6 slots on each wall) are open for standard high-speed full-span model testing, whilst the sidewall slots are closed, achieving an overall effective porosity of 3.4 % (see Fig. 5(a)). For standard high-speed half-span model testing, with the model installed beneath the top wall, the test section has solid top and bottom walls and slotted sidewalls (4 slots on each wall) as shown in Fig. 5(b). The overall porosity for a high-speed half-span model testing is 4.6 %.
A comprehensive control of mass flow between the liquid nitrogen (LN2) injection upstream of the main compressor and the exhaust of gaseous nitrogen (GN2) upstream of the stilling chamber enables to achieve and maintain the desired flow temperature and tunnel pressure level. A simultaneous stopping of LN2 injection and GN2 exhaust results in a gradual increase of gas temperature because of heat generated by the compressor. ETW uses this procedure, the so-called 'temperature step', for high-speed laminar flow testing with the application of TSP measurement to locate the laminar-turbulent transition. During such step, temperature differences on the model surface can be

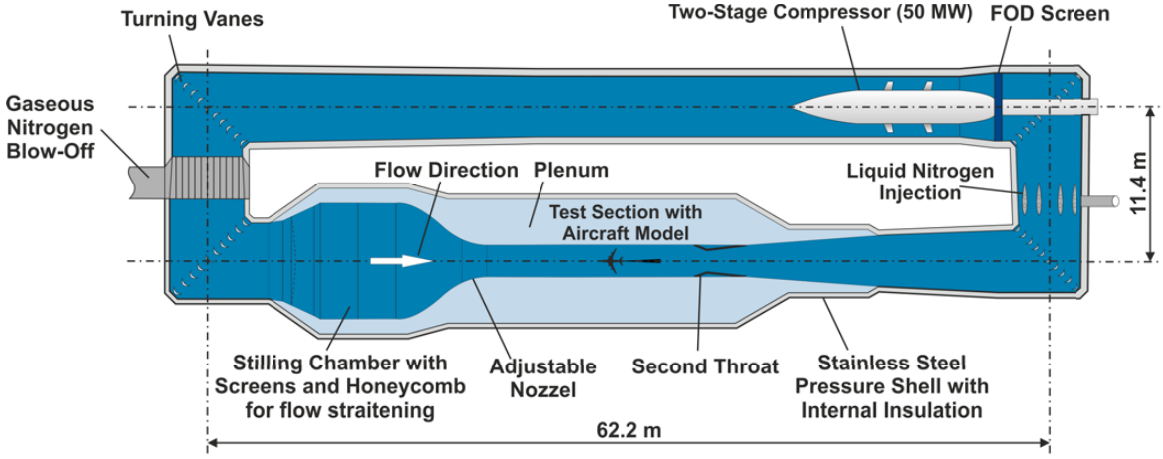


Figure 4 – ETW aerodynamic circuit.

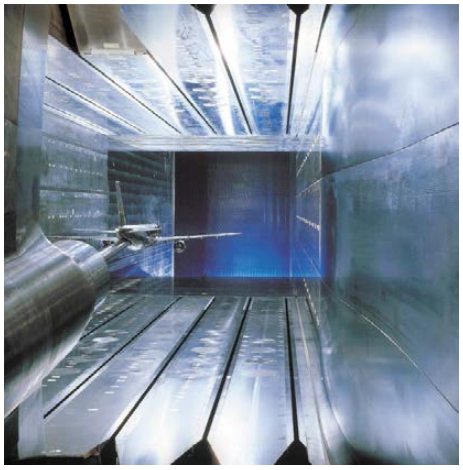

(a) Full-span model wall configuration

(b) Half-span model wall configuration

Figure 5 – ETW's slotted wall configurations.

measured and differentiate between laminar and turbulent covered surfaces as the heat transfer in the surface depends on the boundary layer status. The temperature increase is however kept to a minimum ($\Delta T_t < 10$ K) in order to minimise any changes to the target Mach and Reynolds number during the temperature step [5].

Two filling screens followed by a flow straightener (honeycomb-type) of large depth/cell diameter ratio and two anti-turbulence screens in the stilling chamber, and a large nozzle contraction ratio $(12:1)$ provide the high flow quality in the test volume.

The 50 MW two-stage compressor provides the primary pressure ratio that is required to achieve the desired test-section Mach number. This Mach number control, based on compressor RPM control, is however not capable of an immediate response to a rapid Mach number change in the test section due to its sluggish manner. Therefore, ETW uses a pair of trim flap control devices that are installed on the centre support body in the second throat for fine and quick Mach number adjustment (see Fig. 6). This method, based on drag compensation, is the standard Mach number control procedure at ETW, particularly in the low Mach number range between $M = 0.13$ and $M = 0.65$. At transonic Mach numbers $(0.65 < M < 1.0)$, the trim flap control method can be combined with an adjustable second throat to enable choking downstream of the test volume. The choked flow condition is achieved by a combination of deployment angles between the second-throat wall segments and the trim flaps. This Mach control method allows maintaining quick and stable test-section Mach number and has the benefit of preventing the upstream propagation of any flow disturbances generated in the high-speed diffuser, thus ensuring high flow quality in the test section. More information about ETW can be found in Refs. [6, 7].

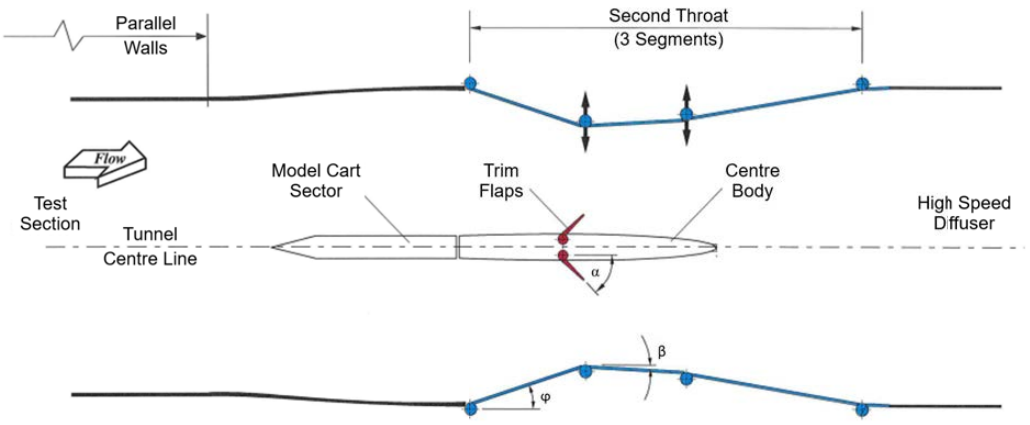


Figure 6 – Schematic of ETW's second throat and trim flap control devices.

## 3. Test Program

The performed flow-quality assessment can be divided into two parts: the first entry used a rotating survey rake (Fig. 7(a)) was conducted in 2019 and the following verification test campaign with a three-arm checkout probe (Fig. 7(b)) was performed in 2021.

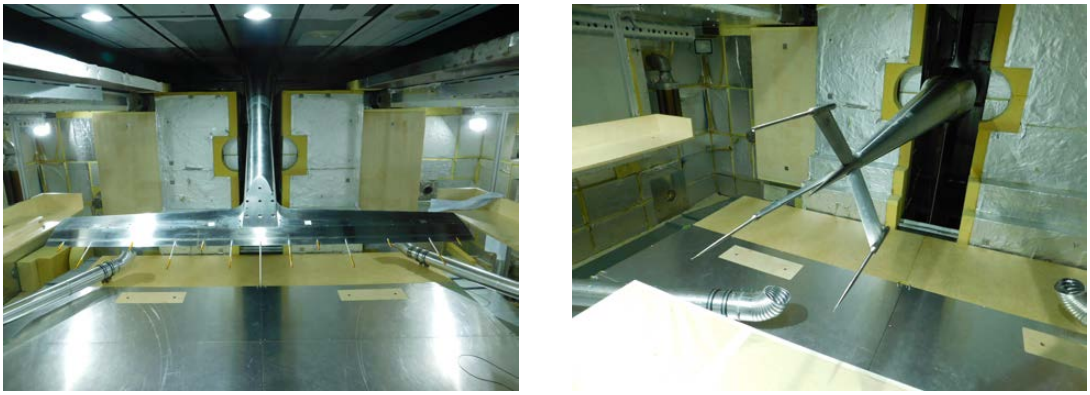

(a) Rotating survey rake (b) Three-arm checkout probe

Figure 7 – Rotating survey rake and three-arm checkout probe in the Variable Temperature Checkout Room (VTCR).

### 3.1 First Test Entry

The main objective of the first entry was to acquire a comprehensive flow-quality reference dataset in the test section as well as the stilling chamber over a substantial range of ETW's operating conditions. A rotating survey rake, equipped with hot-wire probes and unsteady static and unsteady total pressure probes, was used to acquire the comprehensive flow characteristics in the test section. Additional flush-mounted unsteady pressure sensors were installed in the test section sidewalls to support the analysis of the rotating survey rake measurements (see Fig. 8). In order to obtain flow quantities in the stilling chamber, a robust reference sensor was installed. One goal here was to investigate correlations between the flow characteristics in the stilling chamber and the test section. It was further intended that the reference sensor is permanently installed in the top wall of the stilling chamber and available to serve as a kind of transfer standard, and substantiate that the tunnel characteristics haven't changed for a particular future laminar flow test such that previously elaborated spectral characteristics in the test section still apply.

Two different wall slot configurations, representing ETW's standard high-speed full-span and half-span model testing environments, respectively, were tested to evaluate effects of the slotted walls on the test section flow characteristics. For each test section configuration, eight temperature and

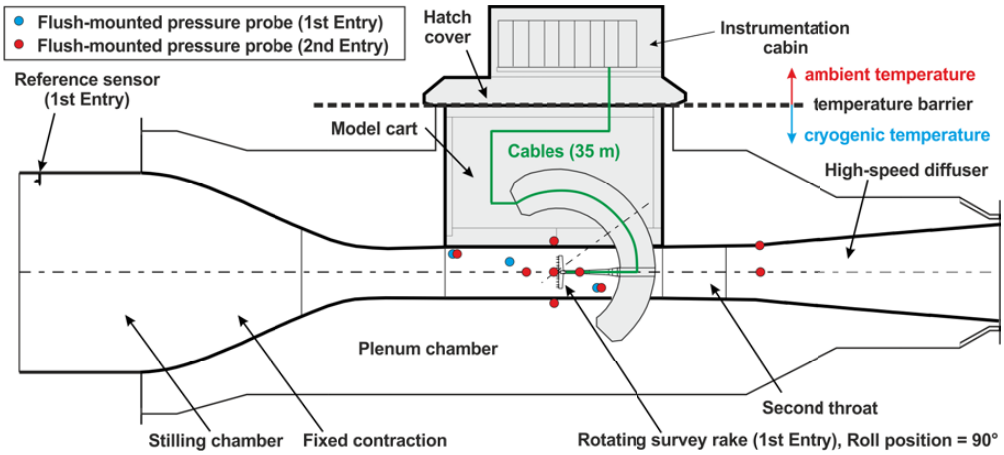


Figure 8 – Location of employed instrumentation components in the tunnel circuit.

| | |
|---|---|
| Test section configurations | Full-span Model (FM) slotted walls<br>Half-span Model (HM) slotted walls |
| Pressure ($P_t$) & Temperature ($T_t$) | 110, 240 kPa @ 280 K<br>110, 445 kPa @ 160 K<br>138, 198, 300, 445 kPa @ 120 K |
| Mach numbers | 0.20, 0.30, 0.50, 0.70, 0.75, 0.80, 0.85, 0.90 (0.95 only for FM) |
| Roll angles ($\varphi$) | FM: 0°, 45°, 90°, 135°, 180°<br>HM: -90°, -45°, 0°, 45°, 90° |

Table 1 – Primary test points of the first FQA entry.

pressure combinations were selected as defined in Table 1. They cover ETW's typical test Reynolds numbers and include coverage for natural laminar flow (NLF) relevant test conditions (see Fig. 9 and Fig. 10). The maximum Reynolds number tested was about 33 million (reference chord of 0.22 m) and 47 million (reference chord of 0.31 m) for the full-span and half-span model slotted configurations, respectively. In total, nine Mach numbers between $M = 0.2$ and $M = 0.95$ (for the half-span model slotted wall configuration up to $M = 0.9$) were selected at each Reynolds number.
Some of test points were specifically chosen to investigate the Reynolds number effects on the empty test-section flow characteristics by holding the dynamic pressure and Mach number constant ((a) in Fig. 10) and to study the dynamic pressure effect by keeping the Mach number and Reynolds number constant ((b) in Fig. 10). The eight combinations of total temperature and total pressure also allow investigating flow phenomena at an identical flow velocity and a comparable Reynolds number, but at a different speed of sound (see Fig. 11). For each combination of Mach number, Reynolds number and test section slot configuration, the survey rake was rotated around the test section centerline with an angle step of 45° to evaluate flow homogeneity across the test section (see Fig. 12).
Beside the primary test points mentioned above, impacts of ETW's Mach number control methods (compressor RPM control, trim flap control and choked second throat in combination with the trim flap control) on the test-section flow characteristics was also studied at transonic Mach numbers (see also Fig. 10 for ETW's performance envelope regarding the Mach number control methods). In addition, the influence of the temperature step method used for the laminar flow testing with the application of TSP technique was investigated at discrete test points.

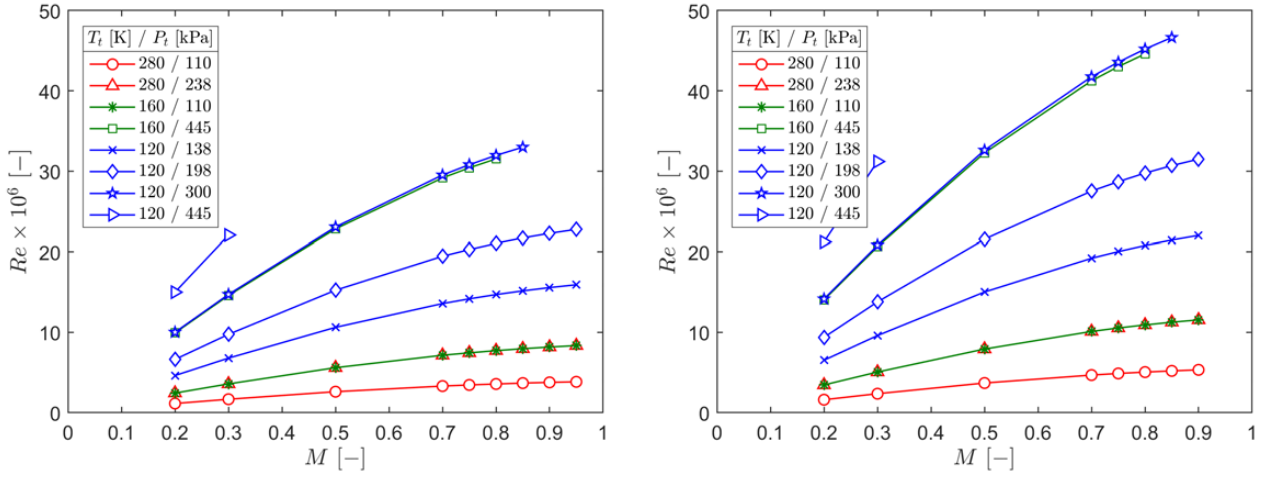


(a) FM wall configuration (ref. chord of 0.22 m) (b) HM wall configuration (ref. chord of 0.31m)

Figure 9 – Test points expressed as tunnel Reynolds and Mach number.

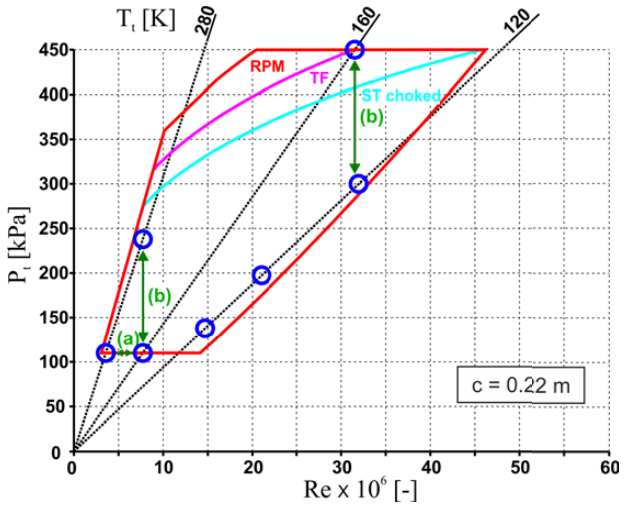


Figure 10 – Test points within ETW's envelope @ $M = 0.8$ for full-span model slotted wall configuration.

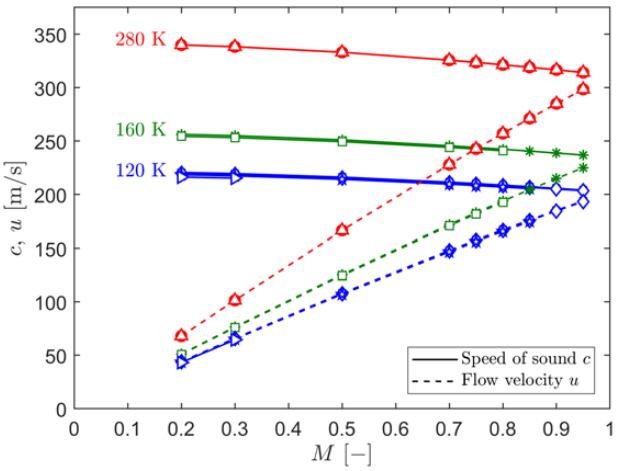


Figure 11 – Tested flow velocity ($u$) and speed of sound ($c$).

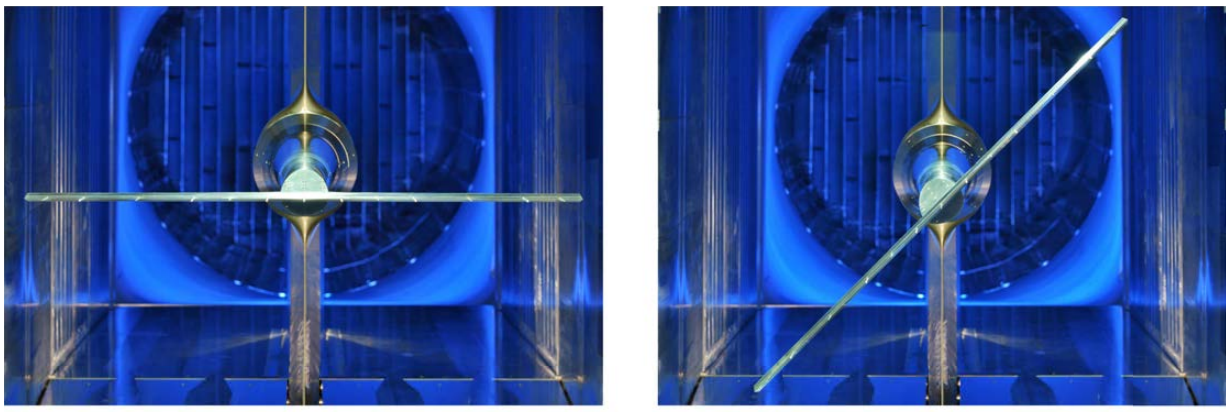


Figure 12 – Rotating survey rake in the test section.

## 3.2 Second Test Entry

After the preliminary analysis of the first entry, a second assessment campaign followed to verify findings obtained from the first FQA entry. The second entry concentrated on understanding the phenomena related to different Mach number control methods. For this purpose, several flush-mounted differential-type unsteady pressure sensors (Kulites) were installed in the test section walls, in the plenum chamber close to the wall slots and in the high-speed diffuser (see also Fig. 8). A three-arm checkout probe equipped with two hot-wire probes and one unsteady total pressure sensor was used to measure flow characteristics near the test section centerline. The second entry was performed only at one temperature-pressure combination (280 K / 110 kPa) and only for the full-span model slotted wall configuration, but with a more refined Mach number grid, as defined in Table 2.

| Control method | Mach number @ $T_t = 280$ K & $P_t = 110$ kPa | |
|---|---|---|
| RPM | [ 0.15, 0.20, 0.30, 0.40, 0.50, 0.55, 0.60, 0.65 ] | [ 0.70, 0.75, 0.80, 0.85, 0.90, 0.95 ] |
| Trim Flap (TF) | [ 0.15, 0.20, 0.30, 0.40, 0.50, 0.55, 0.60, 0.65 ] | [ 0.70, 0.75, 0.80, 0.85, 0.90, 0.95 ] |
| Second Throat choked + TF | | [ 0.70, 0.75, 0.80, 0.85, 0.90, 0.95 ] |

Table 2 – Tested Mach numbers for the second test entry.

## 4. Experimental Details

This section presents a detailed overview of the employed instrumentation components and their calibration.

### 4.1 Rotating Survey Rake

The first entry of the flow quality assessment used a rotating survey rake. The rake was used during ETW's initial calibration and commissioning phases to determine flow characteristics in ETW's empty test section. The survey rake has a double-wedge symmetric profile with a maximum thickness of 26 mm and a span of 1700 mm. The leading edge is unswept, the tip chord is 190 mm and the nominal sweep of the trailing edge is 4°. The survey rake is mounted via an adapter to a straight stub-sting connected to the model cart sting boss and can be rotated around the tunnel centerline with a high precision ($\Delta\varphi < 0.01°$).

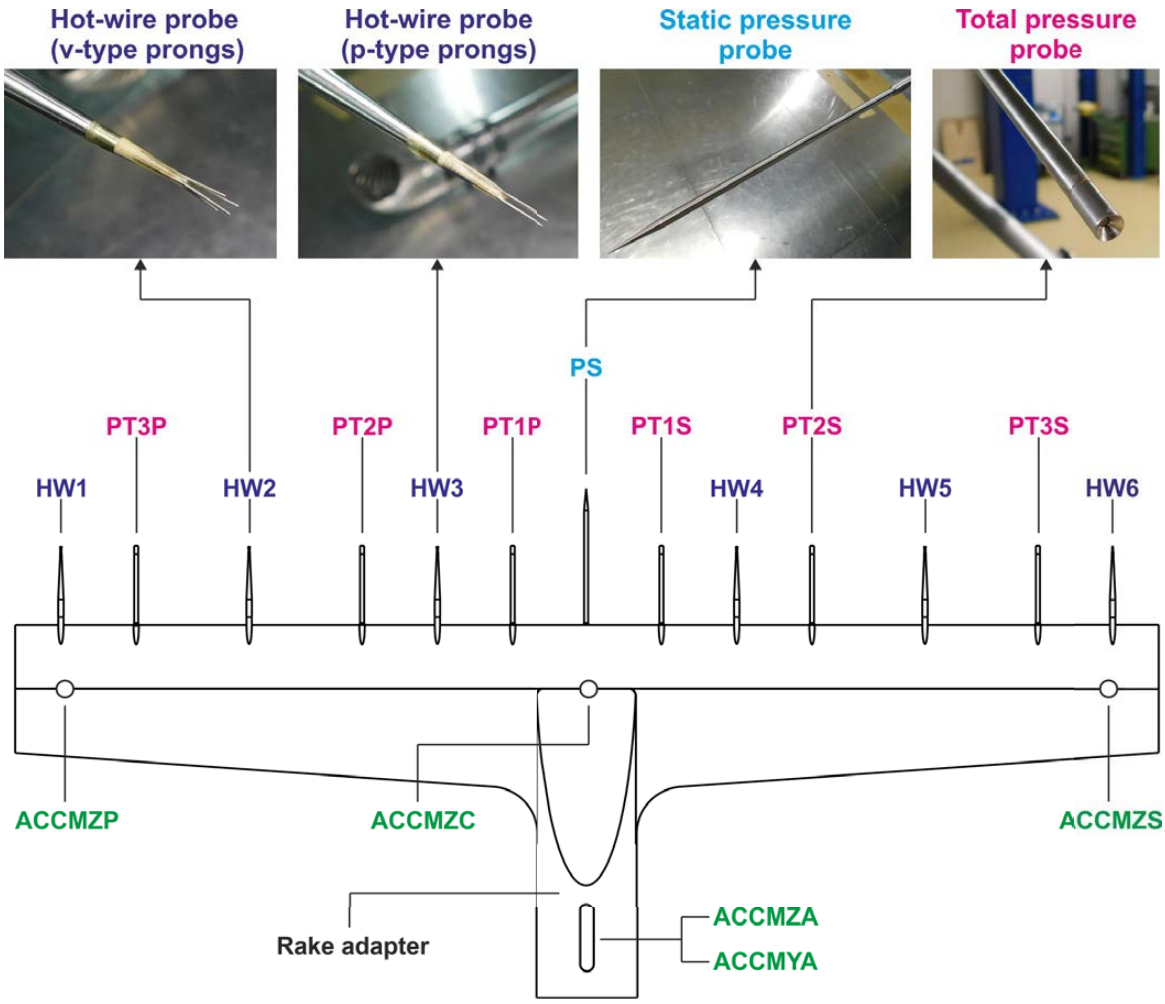


Figure 13 – Rotating survey rake and instrumentation components.

ETW's cryogenic capable Anti-Vibration System (AVS), installed in the straight stub-sting between the rake adapter and the sting boss, cancels out a certain level of low frequency sting Eigen-mode vibrations in two degrees of freedom. Six x-type hot-wire probes and six unsteady total pressure probes are distributed along the span to obtain the spanwise flow characteristics. In addition, a conical pressure probe is mounted on the rake centerline to measure test section static pressure at the point of model rotation. The spanwise locations of the applied probes are presented in Fig. 13. Transition strips were placed close to the leading edge of the rake to avoid laminar separation induced vibrations and/or periodic vortex shedding. To enable detection of setup vibration caused signal components in the hot-wire measurements, the rake's dynamic behaviour was monitored by five accelerometers embedded at different locations in the rake and rake adapter. A 'ping' test of the rake assembly was conducted in the test section after completion of the productive test runs to

establish the dynamic behaviour of both the rake and hot-wires at wind-off conditions. Fig. 14(a) reveals the structural dynamic characteristics of the survey rake obtained from the ping tests with three different impulse positions (rake starboard, port and centre). The vibrations were captured by the accelerometer ACCMZP that is located on the port side and measuring acceleration normal to the wing plane (see also Fig. 13). Fig. 14(b) presents the corresponding anemometer output signals from a hot-wire, located also on the port side close to the ACCMZP. The comparison between the accelerometer and the hot-wire readings at the wind-off condition clearly indicates a significant response of the hot-wire readings due to the rake vibration.

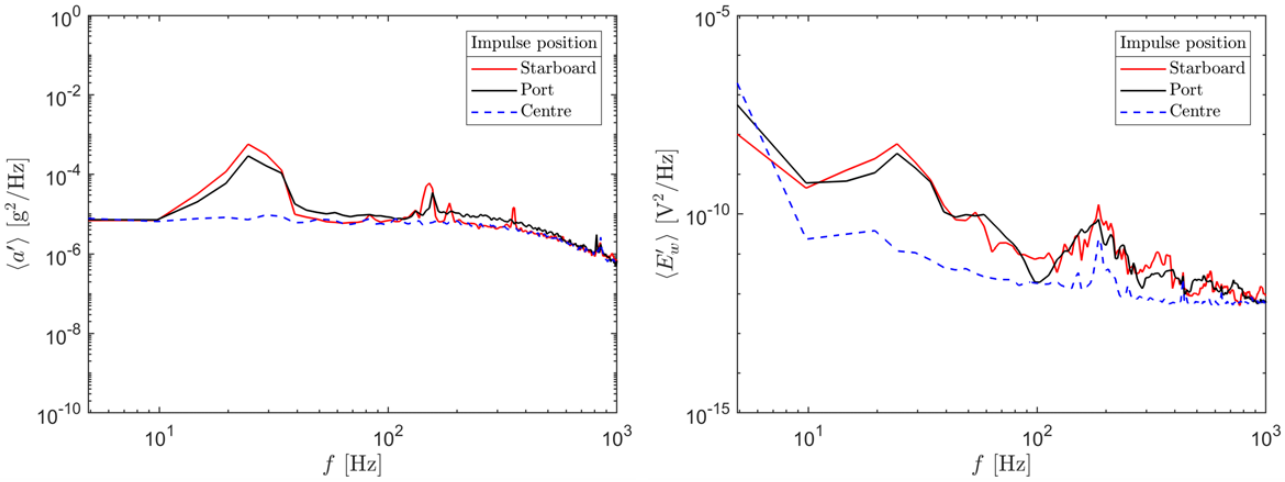


(a) Accelerometer ACCMZP

(b) Hot-wire HW1 (wire A)

Figure 14 – Wind-off ping test @ $T_t = 296$ K.

## 4.2 Three-arm Checkout Probe

In order to investigate flow characteristics close to the test section's centerline, ETW's three-arm checkout probe was used in the second FQA entry. This probe was also constructed and used during the ETW's initial calibration and commissioning phases. The checkout probe has three support arms with an angular separation of 120°. To minimise any stagnation influence, a conical extension is included in the centre of the probe, as shown in Fig. 15. In the second FQA entry, two hot-wire probes (one with v-type prongs and one with p-type prongs) and one total pressure probe, used in the first FQA entry, were installed on the checkout probe. In addition, one vertical accelerometer and one lateral accelerometer were placed in the probe to enable monitoring of the dynamic behaviour of the checkout probe. The checkout probe can be rotated around the sting axis, however, only a fixed roll position ($\varphi = 0°$) was considered during the second FQA entry.

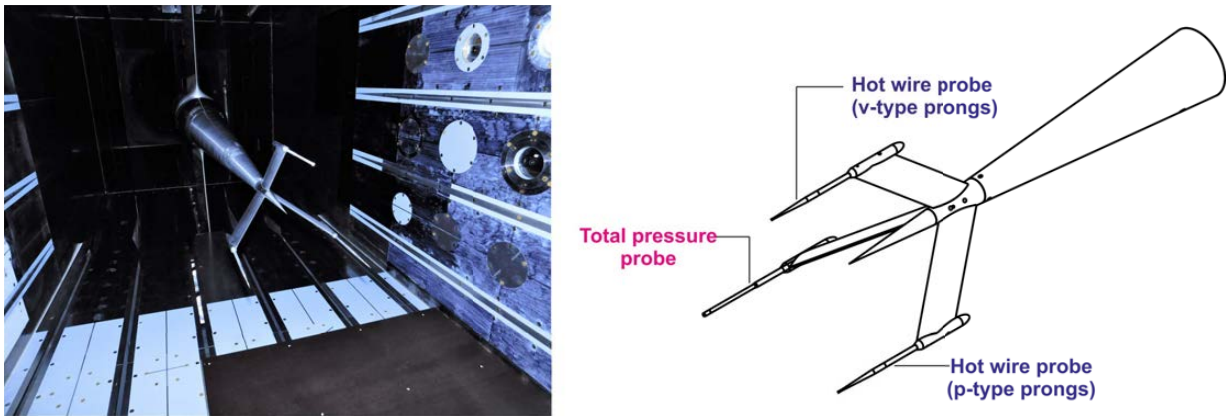


Figure 15 – Three-arm checkout probe and instrumentation components.

### 4.3 Reference Sensor

In order to obtain flow quantities in the stilling chamber, a reference sensor was manufactured and installed on the top wall of the stilling chamber. The sensor's total height was determined to ensure that the sensor measures the flow field outside the stilling chamber's boundary layer. As the sensor should be installed permanently and support future laminar flow test campaigns, hot-film probes were selected due to their high survivability. To support the hot-film calibration, the reference sensor also includes one temperature sensor (type Pt100), one unsteady absolute-type total pressure transducer as well as one static pressure transducer. In addition, a differential-type pressure transducer is connected between the total and static pressure tubes to measure dynamic pressure (see Fig. 16). All pressure transducers used for the reference sensor were non-temperature compensated type and in general not compatible with cryogenic applications. Therefore, a comprehensive insulation and heating system was installed to provide thermal isolation of the transducers from the cryogenic test environment and thus ensuring that the reference probe instrumentation operates at nominally ambient conditions.

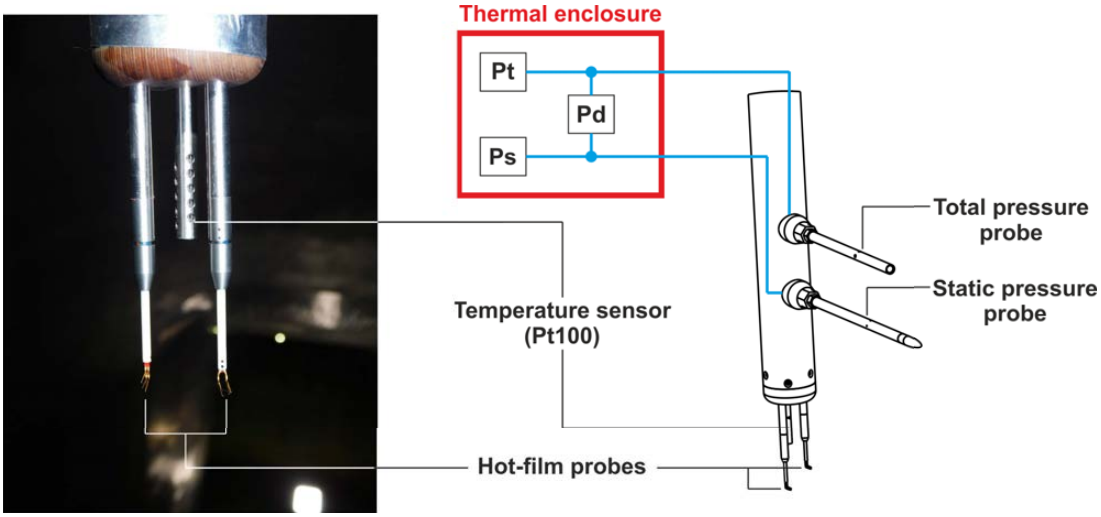


Figure 16 – Reference sensor in the stilling chamber.

$$M = \sqrt{\frac{2}{\kappa - 1}\left[\left(\frac{P_t}{P_s}\right)^{\frac{\kappa-1}{\kappa}} - 1\right]}, \quad \kappa = 1.4 \tag{1}$$

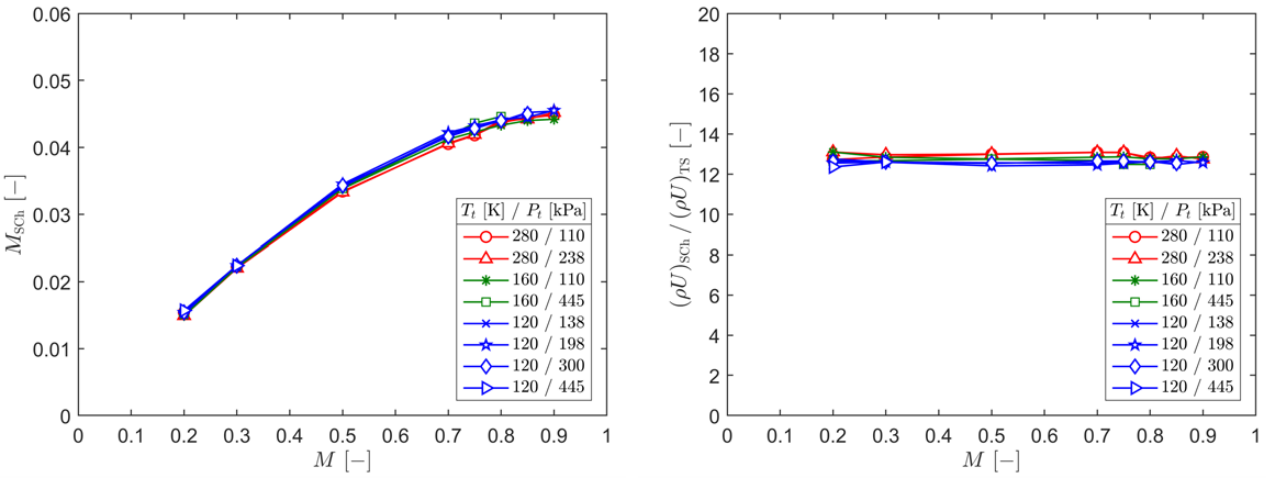


(a) Stilling chamber Mach number

(b) Mass flow ratio

Figure 17 – Results of reference sensor readings as a function of test-section Mach number.

Fig. 17(a) shows the stilling chamber Mach numbers, derived from the reference sensor readings and by using Eq. (1), as a function of the test-section Mach number for all eight tested temperature and pressure combinations. All Mach curves of the cryogenic test conditions coincide with the Mach curves for the test conditions of 280 K, indicating that the thermal enclosure concept works properly. In Fig. 17(b), the reference sensor readings are compared by means of mass flow rate with the readings of ETW's Flow Reference System (FRS), measuring the fundamental flow quantities at the entry of the test section. As expected, the mass flow ratio between the stilling chamber and test section is constant over the entire tested Mach number, as all FQA campaigns were conducted with a fixed nozzle contraction ratio. The measured ratio is however slightly higher than the theoretical value ($A_{SCh} : A_{TS} \approx 12 : 1$).

## 4.4 Velocity Fluctuation Measurements

Hot-wire and hot-film probes were used to measure flow velocity fluctuations in the test section and in the stilling chamber, respectively. Application of the hot-wire measurement in ETW's harsh testing environment (cryogenic conditions and high dynamic pressures), and requiring relatively long cable lengths between the probe and the anemometer bridge circuit represents a special challenge. Therefore, ETW investigated and qualified the use of the hot-wire anemometry technique under ETW's test conditions in previous studies, as described in Refs. [8, 9]. Thereby, the comprehensive behaviour of hot-wire probes was extensively studied over ETW's complete operating envelope in ETW's pilot facility (Pilot European Transonic Windtunnel, PETW). The studies confirmed the applicability of the hot-wire anemometry technique under the cryogenic and high dynamic pressure conditions, but also showed that the application requires special adjustments of the anemometer setup as well as the calibration to achieve high quality velocity fluctuation measurements.

### *4.4.1 Hot-wire Anemometry*

Velocity fluctuations in the test section were measured by using the hot-wire probes in combination with a constant temperature anemometer (CTA). The planning, calibration, performing and data analysis of hot-wire measurements were supported by the project partner from the department of engine acoustics of the Institute of Propulsion Technology at the German Aerospace Centre (Deutsches Zentrum für Luft und Raumfahrt, DLR).


Figure 18 – X-type hot-wire probe.

The adopted hot-wire probes have a x-type wire arrangement to ETW's and DLR's own design. This probe design allows simultaneous measurements of two dimensional unsteady flow fields. Each hot wire detects their effective cooling velocity ($U_{wA}$ and $U_{wB}$) that depends on both the magnitude and the direction of the incoming flow field as well as the wire inclination angle, as shown in Fig. 18. The wire inclination angle $\alpha_w$ and $\beta_w$ then allows converting the measured wire cooling velocities to the actual axial and lateral velocity components of the incoming flow.

Due to the harsh test environment, particularly the high dynamic pressures, wires with a diameter of 9 $\mu$m were chosen to ensure maximum survivability, but at the expense of a reduced response at higher frequencies. The tungsten wires had a nominal length of 2.8 mm. In order to overcome the shrinking of wires under cryogenic test temperatures, the wires were welded onto two needle-type prongs with a little slack. Two types of prong designs were used, the v-type and the p-type prongs (see also Fig. 13). Due to its v-shape arrangement, the v-type prong design was expected to be less susceptible to vibration compared to the conventional p-type prong design.

The distance between the hot-wire probes exposed under cryogenic conditions and the instrumentation cabin, where the anemometer is located at ambient temperature, is about 35 metres (see also Fig. 8). Therefore, the cable can be subjected to large temperature differences (up to $\Delta T_t = 173$ K). For this reason, a cryogenic suitable CAT-7 cable with 4 twisted pairs of wires was used. Two pairs

were used for the dual hot-wire sensors, whilst two pairs are short-circuited at their ends with the purpose of achieving a real-time, automatic temperature compensation of the cable that is subject to a floating resistance because of large temperature changes.
The acquisition of the hot-wire signals was achieved by use of DLR's HDA5 constant temperature anemometry. Due to the reasons mentioned above (long cable and temperature compensation of the cable), a symmetrical $1:1$ bridge configuration was adopted. The anemometer output was acquired by ETW's high-speed data acquisition system at a sample rate of 80 kHz for a duration 10 seconds at each measurement point.
In order to avoid any early failures of the hot-wire probes, particularly at test points with high dynamic pressures, the test program was adapted, so that the test points with low Mach numbers (up to $M = 0.7$) were performed first. After these measurement points were successfully completed, the test campaign continued with the higher Mach numbers up to 0.95. Despite these measures, some hot-wires failed particularly at high tunnel pressures and high Mach numbers. During the reconfiguring of the test section for the second test configuration (half-span model slotted wall configuration) the defective probes were either exchanged or repaired.
The hot-wire calibration and productive measurement in the second FQA entry were conducted by use of ETW's Dantec StreamLine Pro constant temperature anemometer with four installed anemometer units operated in a symmetrical $1:1$ bridge configuration. Except for the anemometer itself, the cables were identical, and the hot-wire probes and measurement setup used during the first FQA entry were maintained for the second entry (see Table 3).
Spectral analysis of the hot-wire data from the first entry indicated some unexpected dynamic behaviour potentially caused by probe vibrations (see Fig. 19(a)). Therefore, additional verification tests were performed with the support of the Chair of Aerodynamics and Fluid Mechanics (AER) at the Technical University of Munich (TUM). The dynamic behaviour of all hot wire probes was identified by use of a low turbulence Dantec hot-wire calibrator (see Fig. 19(b)). Table 3 shows the hot-wire measurement setup of three different tests, indicating that only the hot wire support and prongs were identical between each test campaign. A comparative analysis reveals that the observed dynamic behaviour of the hot-wire signals is mainly related to the flow induced vibration of the hot-wire sup-

| Test Name | Support & Prongs | Wires | Anemometer | Bridge ratio | Rake | Cable length | $T_t$ | Wind source |
|---|---|---|---|---|---|---|---|---|
| FQA-1.Entry | original | original | DLR-HDA5 | $1:1$ | Rotating rake | 25 m | 280 K | ETW |
| FQA-2.Entry | original | repaired | ETW-Dantec | $1:1$ | Checkout probe | 25 m | 280 K | ETW |
| AER-TUM | original | repaired | ETW-Dantec | $1:20$ | Dantec support | 5 m | 293 K | Dantec Calibrator |

Table 3 – Tested Mach number for the second test entry.

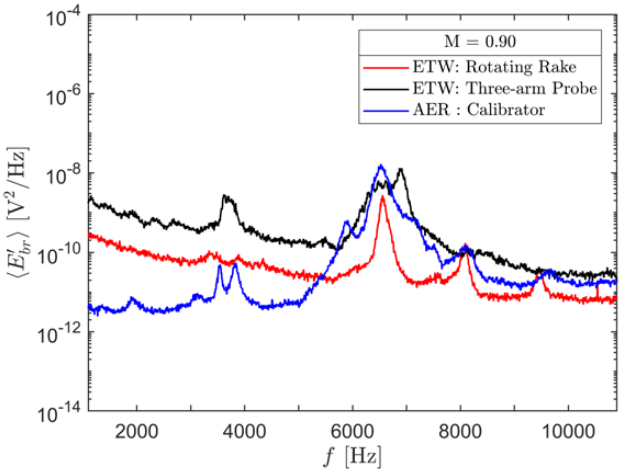


(a) PSD of bridge outputs

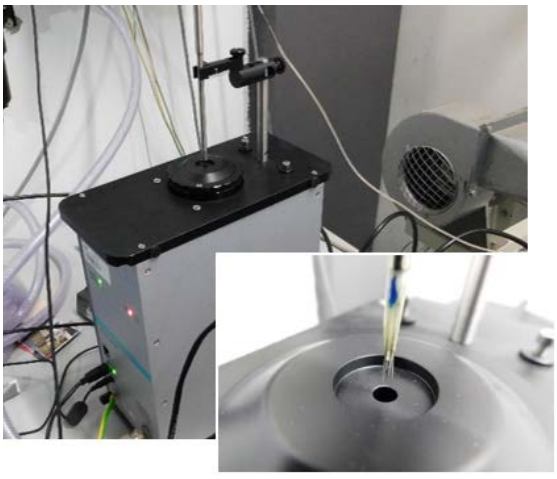

(b) Hot-wire calibration facility at AER, TUM

Figure 19 – Comparative analysis of probe-specific dynamic behaviour.

port and prongs, and not due to the employed measurement setups as well as not due to the flow itself.

### 4.4.2 Hot-film Measurements

Two dual-sensor x-type fiber-film Dantec hot-film probes were placed in the stilling chamber to measure flow quantities upstream of the wind tunnel nozzle (see also Fig. 8 and Fig. 16). The quartz fiber is deposited with nickel film and has a diameter of 70 $\mu$m (except for a quartz coating of approximately 0.5 $\mu$m) with a sensitive film length of 1.25 mm [10]. One hot-film probe (55R53, Fig. 20(a)) measures the flow components $u$ and $v$, while the other hot-film (55R54, Fig. 20(b)) captures the $u$ and $w$ components of the unsteady flow fields. The Dantec StreamLine Pro CTA in symmetrical $1:1$ bridge configuration was used. Except for the anemometer, all measurement setups, including cables, wiring concepts and anemometer setups, were kept identical to the setup for the hot-wire measurements.

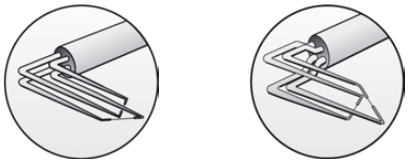

(a) 55R53 (b) 55R54

Figure 20 – Hot-film probes [10].

### 4.4.3 Calibrations

Conventional calibrator based procedures were not applicable to both hot-wire and hot-film probes prior to the test entry mainly because of the huge testing temperature and pressure variations. Therefore, the probes were calibrated 'in-situ' during the measurements in the tunnel. In order to compensate the temperature, static pressure and Mach number influences, the calibration was performed by evaluating the relation between the wire Reynolds $Re_w$ and Nusselt number $Nu$. The Nusselt number describes in general the relation between the heat transfer and heat radiation and can be calculated for the hot-wire application by using the mean wire voltage $E_w$, the wire resistance $R_w$, the wire length $l_w$, the thermal conductivity of flow $\lambda_\infty$, the wire temperature $T_w$ and the local recovery temperature $T_{rec}$, as given in Eq. (2). The Reynolds number of each wires is then determined with the wire diameter $d_w$ and the individual effective cooling velocity $U_w$ with an assumption that there is no lateral velocity component present (see Eq. (3)).

$$Nu = \frac{E_w^2}{R_w \cdot \pi \cdot l_w \cdot \lambda_\infty \cdot (T_w - T_{rec})} \tag{2}$$

$$Re_w = \frac{U_w \cdot \rho_\infty \cdot d_w}{\mu_\infty} \tag{3}$$

Calibration coefficients for each wire are then derived by adopting King's law, as given in Eq. (4).

$$Nu = A + B \cdot Re_w^n \tag{4}$$

Using the calibrations coefficients $A$ and $B$, the actual wire cooling velocity is calculated as follows:

$$U_w = \left[ \frac{E_w^2}{R_w \cdot \pi \cdot l_w \cdot \lambda_\infty \cdot (T_w - T_{rec}) \cdot B} - \frac{A}{B} \right]^{\frac{1}{n}} \cdot \frac{\mu_\infty}{\rho_\infty \cdot d_w} \tag{5}$$

In Fig. 21, the measured total temperature and the calculated recovery and static temperature of three test temperature conditions are compared as a function of the tunnel Mach number. Because of low gradient of the recovery temperature against the Mach number change, DLR preferred the static temperatures to be used for the calibration process, in order to increase the calibration sensitivity particularly at high Mach numbers.

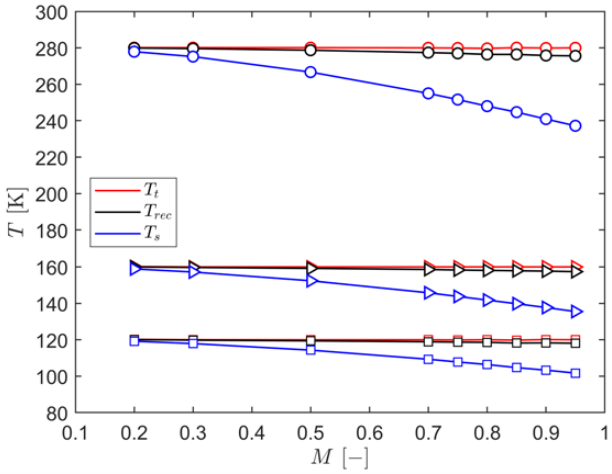


Figure 21 – Total, static and turbulent recovery temperature as a function of Mach number.

In Fig. 22 , the conventional calibration using the wire voltage and the flow velocity is compared with the Nusselt-Reynolds number relation, applied in the present work for all tested temperature and pressure combinations of the first entry. In the present work, calibrations were conducted, when the test condition ($P_t$ or $T_t$) and test section configuration has been changed, resulting in a total of 30 calibrations during the first FQA entry. The classical approach shows that the hot-wire calibration is strongly affected by the flow temperature, tunnel pressure and Mach number. Significant changes in the behaviour of the wire voltage is observed at the high Mach numbers, where the anemometer output seems to be insensitive to the Mach number change (see Fig. 22(a)). Considering the Nusselt-Reynolds number relation, it can clearly be seen that all calibration curves of the identical tunnel pressures coincide and show a good linear ratio, also in the high-speed range. However, the temperature effects are still observed. Previous studies [8, 9] indicated that the temperature effects can be further corrected, resulting in an evaluation of the global coefficients. However, this correction was not applied in the present work.

## 4.5 Pressure Measurements

Steady and unsteady pressure measurements were performed at several locations around the tunnel circuit and at the rotating rake. The most important steady pressure measurement systems are ETW's two Flow Reference Systems (FRS). Beside of total temperature measurement units, each FRS consist of two absolute and two differential pressure sensors of different ranges and accuracies. FRS is the core of ETW's tunnel control, ensuring the correct tunnel flow conditions and being a reference for all other pressure measurements performed within the test section.

Absolute-type pressure transducers used for the reference sensor described in section 4.3 as well as for some flush-mounted unsteady pressure probes on the test-section walls were calibrated 'in-situ' using FRS as the reference at wind-off conditions and for all tunnel temperatures considered during FQA. As shown in Fig. 23(a), the non-temperature compensated type transducer reveals no sensitivity changes, albeit at different tunnel temperatures, as it is isolated by the comprehensive thermal enclosure system from the cryogenic testing environments and therefore operating nominally under ambient temperature conditions. As expected, the temperature compensated type transducer also shows no significant sensitivity change between three tunnel temperatures tested. Small offset changes were however observed and taken into account.

Six total pressure probes and one static pressure probe installed at the rotating rake employed cryogenic compatible, differential-type unsteady miniature pressure transducers. The reference side of these sensor was tided linked to a large volume reservoir whose pressure is also measured by a dedicated steady measurement equipment. The total pressure probes have a special design using a 90 degree inlet cone to make it less sensitive to vibration issues (Fig. 23(b)). The static probe holds a centered sensor sitting close to the four equally distributed surface pressure tabs on the probe body.

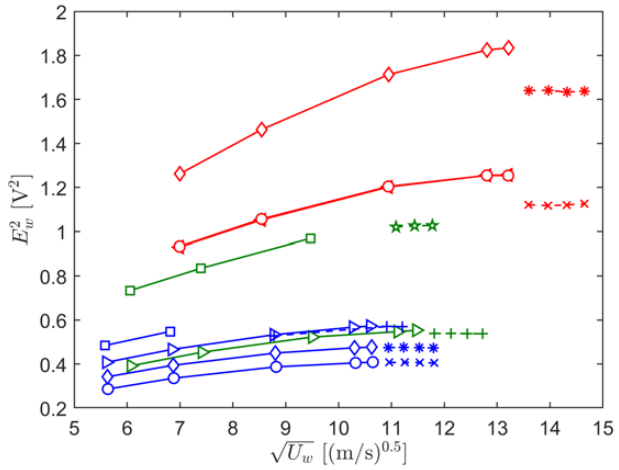


(a) HW6 (wire B): Mean wire voltage over effective cooling velocity

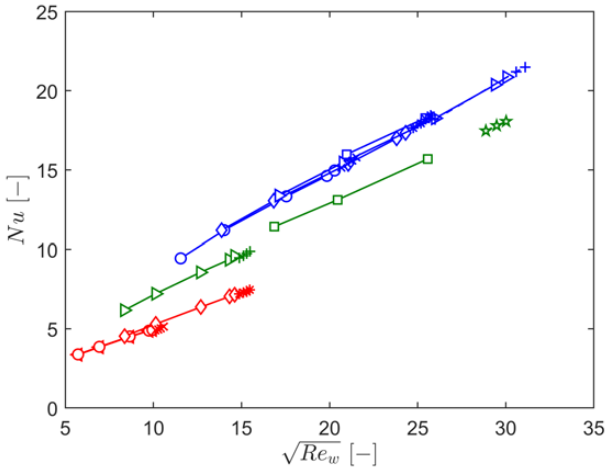


(b) HW6 (wire B): Nusselt number over wire Reynolds number

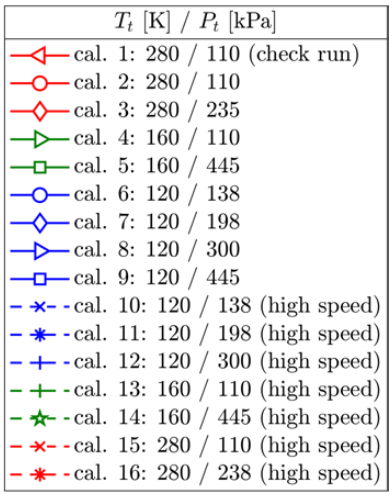


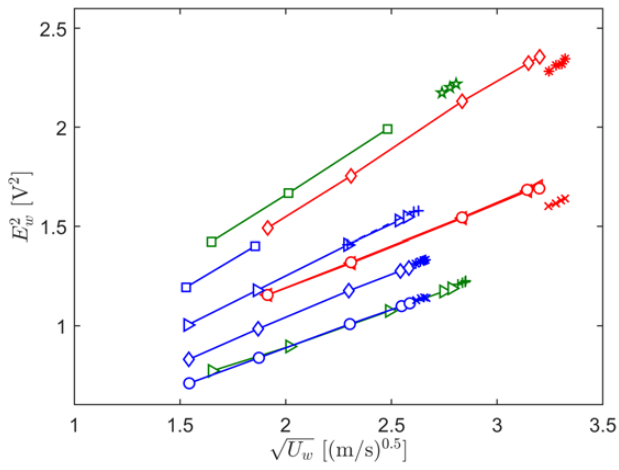


(c) HF1 (wire B): Mean wire voltage over effective cooling velocity

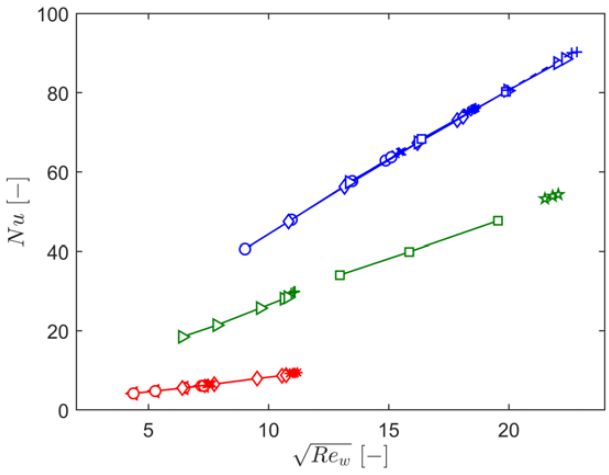


(d) HF1 (wire B): Nusselt number over wire Reynolds number

Figure 22 – Comparison of calibration curves (full-span model slotted configuration and rake roll position $\varphi = 0°$).

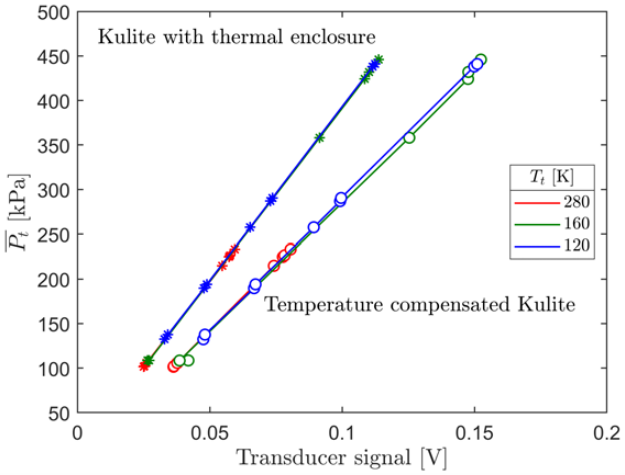


(a) Calibration of absolute-type pressure tranducers

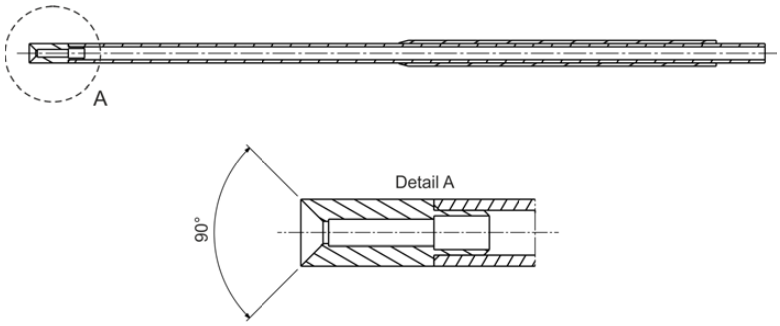


(b) Rake total-pressure probe design

Figure 23 – Pressure measurements.

## 5. Results

This section presents results of the primary data analysis. The focus lies thereby on the evaluation of effects of the ETW's different slotted test-section wall configurations as well as of the Mach number control methods on the test-section flow characteristics.

The work aims to provide spectral characteristics of the flow to be used for computational purposes, e.g. transitional boundary layer receptivity, buffet or dynamic aeroelastic analysis. Therefore, the measured data were cleaned from sensor setup related artifacts e.g. hot-wire prong or support or rake vibrations using notch filters, and band-pass filtered between 10 Hz and 30,000 Hz (Butterworth, second order). The integral fluctuation values shown result from integrating the cleaned power spectral density.

### 5.1 Slotted Wall Configurations

Fig. 24 presents two different test-section wall configurations including the rotating survey rake and its instrumentation components, employed for the first FQA entry. Each roll position ($\varphi$) represents the standard test section configuration for a full-span and half-span model testing, respectively. Due to the rectangular shape of the test section, the distance between the outboard probe and the wall surface at the rake roll position of $\varphi = 0°$ are not the same as at $\varphi = 90°$. Therefore, the outboard probes (PT3P, PT3S, HW1 and HW6) are expected to be stronger affected from the slot flow with a higher level at the rake roll position $\varphi = 90°$. Note that both the number and width of opened slots are also different between the test-section wall configurations.

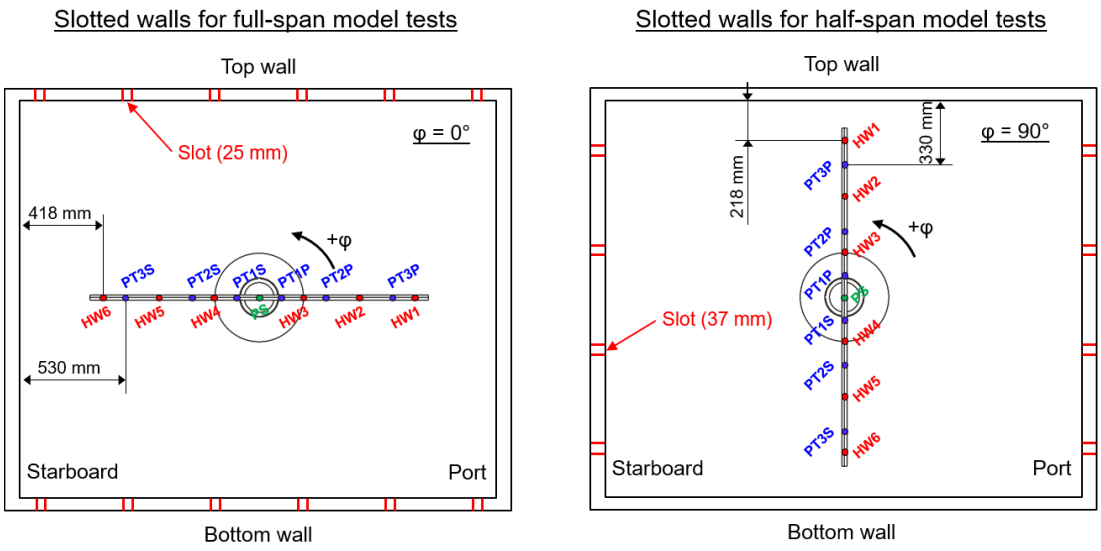


Figure 24 – Schematic of slotted test-section wall configurations.

### *5.1.1 Pressure Fluctuations*

**Static pressure fluctuations in the test section centerline** In Fig. 25(a), static pressure fluctuations for the FM wall configuration are given as a function of the test-section Mach number for all eight tested temperature-pressure combinations for the typical roll position of a standard full-span model testing ($\varphi = 0°$). The data were obtained from the unsteady static pressure probe (PS) mounted in the middle of the rotating survey rake. Because the rake wing has a symmetrical profile and zero rake incidence was tested, it could be assumed that the probe measures static pressure field of the quasi-empty test section at the point of model reference. With increasing Mach number and thus decreasing tunnel static pressure, $\langle P_s' \rangle / \overline{q}$ globally tends to have lower levels in the test section centerline. Differences of fluctuation levels between the high and low tested Reynolds numbers at a same Mach number also decrease with increasing flow speed. The differences then become negligible at the high test-section Mach numbers ($M > 0.70$). It might be the result of on the one hand due to the fact that in this high-speed regime the proportion of dynamic pressure is more dominant, and on the other hand, in the high Mach number range ($M > 0.70$), ETW uses a combined method of the trim flap control and the second throat choked to achieve and maintain the desired test-section Mach number. The use of the choking second throat ensures preventing the upstream propagation

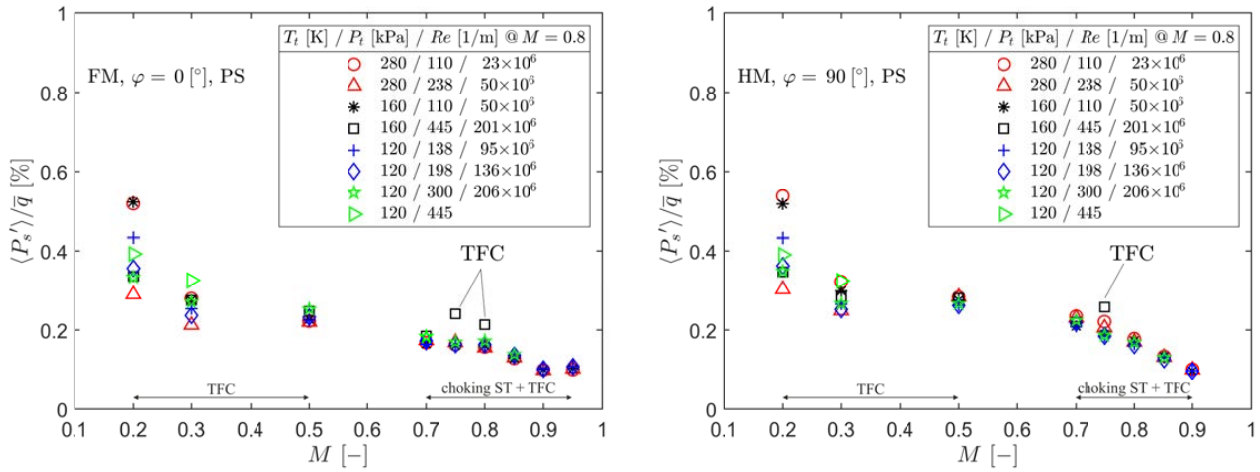


(a) FM wall configuration, $\varphi = 0°$

(b) HM wall configuration, $\varphi = 90°$

Figure 25 – Static pressure fluctuations in the test section centerline (TFC = Trim Flap Control, ST = Second Throat).

of disturbances from the high-speed diffuser region to the test section (see Sec. 5.2). High levels of fluctuation indicated with 'TF' in Fig. 25(a) are because these test points were tested only with the trim-flap control (TFC) method (see also Fig. 10).
Fig. 25(b) presents the static pressure fluctuations for the half-span model wall configuration for a typical right-hand wing configuration ($\varphi = 90°$). Both the characteristics and levels are comparable with the full-span model test points. Again, at the test points indicated with 'TF' in Fig. 25(b), the second throat was not choked.

**Total pressure fluctuation spatial homogeneity** Fig. 26 presents lateral and angular distributions of total pressure fluctuation, measured by six unsteady total pressure transducers on the survey rake, at different angular positions for a low ($M = 0.3$) and high Mach number ($M = 0.9$) as well as for low and high Reynolds number test-point, respectively. At the high Mach number ($M = 0.9$), the outboard pressure probes (PT3P and PT3S) measure higher total pressure fluctuations, if they are located close to the wall slots ($\varphi = 90°$ for the FM test case and $\varphi = 0°$ for the HM wall configuration). Due to the shorter distance between the outboard probes and the slotted walls ($\Delta l_t = 200$ mm), fluctuation levels near the slotted walls are more significant for the FM test than the HM test case. As expected, all results of measurements using the inboard probes (PT2P, PT1P, PT1S and PT2S) do not show any significant angular dependencies and have similar fluctuation levels to each other, indicating the homogeneous total pressure distributions in the core region of the test volume. The outboard probes show a similar fluctuation levels as the inboard probes, if they are not subject to the slot flow ($\varphi = 0°$ and $\varphi = 180°$ for the FM test case and $\varphi = -90°$ and $\varphi = 90°$ for the HM wall configuration). In general,

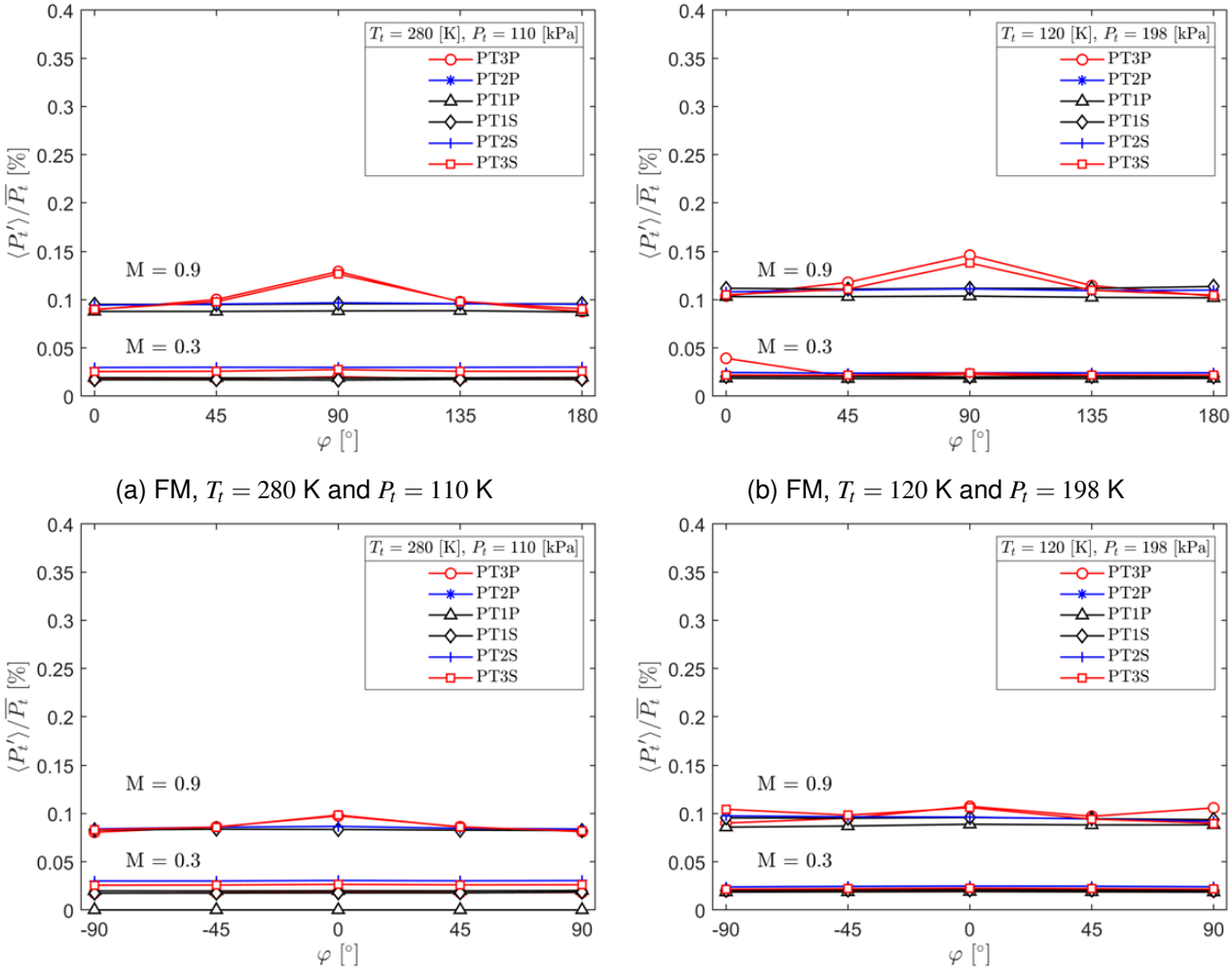


(a) FM, $T_t = 280$ K and $P_t = 110$ K

(b) FM, $T_t = 120$ K and $P_t = 198$ K

(c) HM, $T_t = 280$ K and $P_t = 110$ K

(d) HM, $T_t = 120$ K and $P_t = 198$ K

Figure 26 – Lateral and angular distributions of fluctuating total pressure.

the results indicates a homogeneous lateral total pressure distributions across the test section.
At the low Mach number ($M = 0.3$), the outboard probes do not show any significant growth of the total pressure fluctuation near the slotted walls. The fluctuation levels lie below 0.05 % of the mean test-section total pressure.

**Influences of Mach number** The Mach number dependency of the total pressure fluctuations is presented in Fig. 27 and Fig. 28 for the inboard probe (PT1S) and outboard probe (PT3P), respectively. In contrast to the static pressure fluctuation, the total pressure fluctuation, measured by the probe PT1S that is located close to the tunnel centerline, grows with increasing Mach number up to $M = 0.5$ for the high Reynolds number test-points and $M = 0.7$ for the low Reynolds number test points. Beyond these Mach numbers, the fluctuation levels decrease with the growing Mach number. The influence of the trim-flap control method on the total pressure fluctuations are also visible at the high Mach numbers (see Fig. 27(a) and Fig. 27(b)). In contrast to the inboard probe, the results of the outboard probe measurements (PT3P) indicate a clear dependency on the Mach number (see Fig. 28(a)). If the flow speed increases, the tunnel static pressure decreases which in turn increases the difference of the static pressure between the test section and the plenum. As a result, it might lead to a more significant slot flow and increasing total pressure fluctuation in the region of slots.

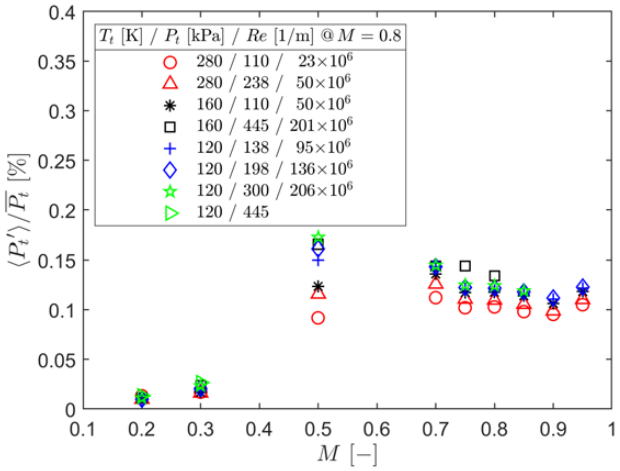


(a) Standard FM roll position at $\varphi = 0°$

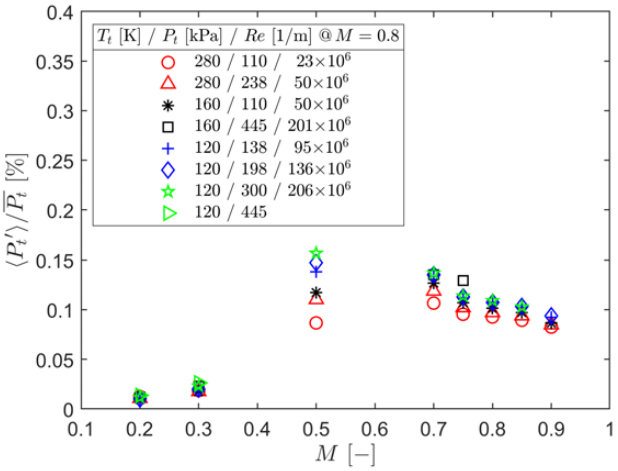


(b) Standard HM roll position at $\varphi = 90°$

Figure 27 – Total pressure fluctuations near the tunnel centerline (inboard probe PT1S).

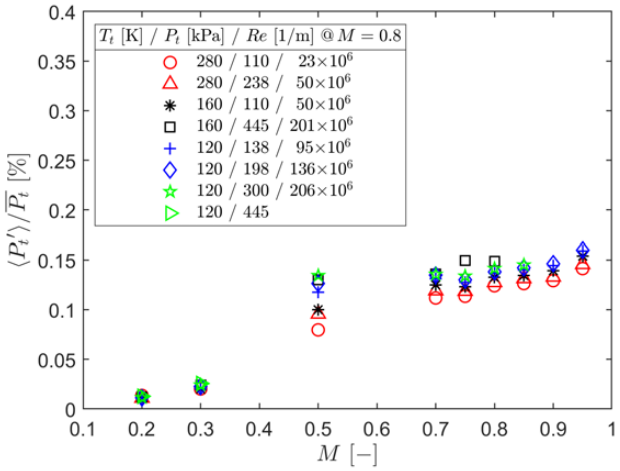


(a) FM wall configuration, $\varphi = 90°$

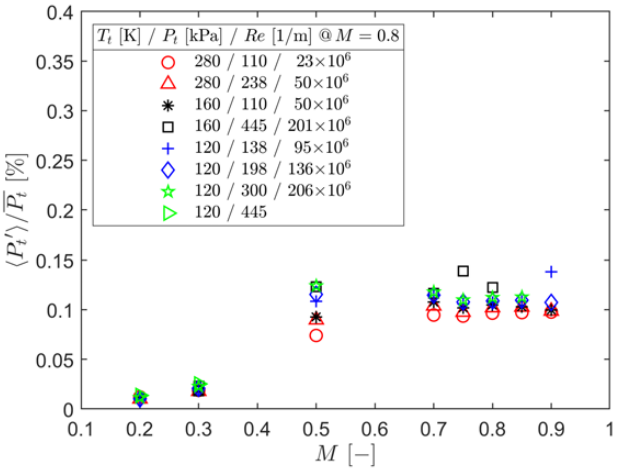


(b) HM wall configuration, $\varphi = 0°$

Figure 28 – Total pressure fluctuations near slotted walls (outboard probe PT3P).

**Solid wall influences** Total pressure fluctuations, measured by the outboard probe PT3P in the region of the FM slotted top wall, are compared with the fluctuations gathered during the HM test case at the same roll position ($\varphi = 90°$) and given in Fig. 29(a). Because the top and bottom slots were closed, the results at the rake roll position $\varphi = 90°$ for the HM wall configuration represent the total pressure fluctuation observable at a closed wall test section configuration. As outlined above, the total pressure fluctuation near the slot flow grows with increasing Mach number, while the level measured near the solid wall is rather stagnant. Both fluctuation levels and characteristics of the outboard probe for the solid wall case are comparable with those of the inboard probe, showing that the solid walls do not have any significant effects on the total pressure field at the position of the outboard probe. The same analysis can be applied to the HM test case with the opened sidewall slots, as given in Fig. 29(b). The result reveals that at the position of the outboard probe the influence of both solid and slotted sidewalls is not significant.

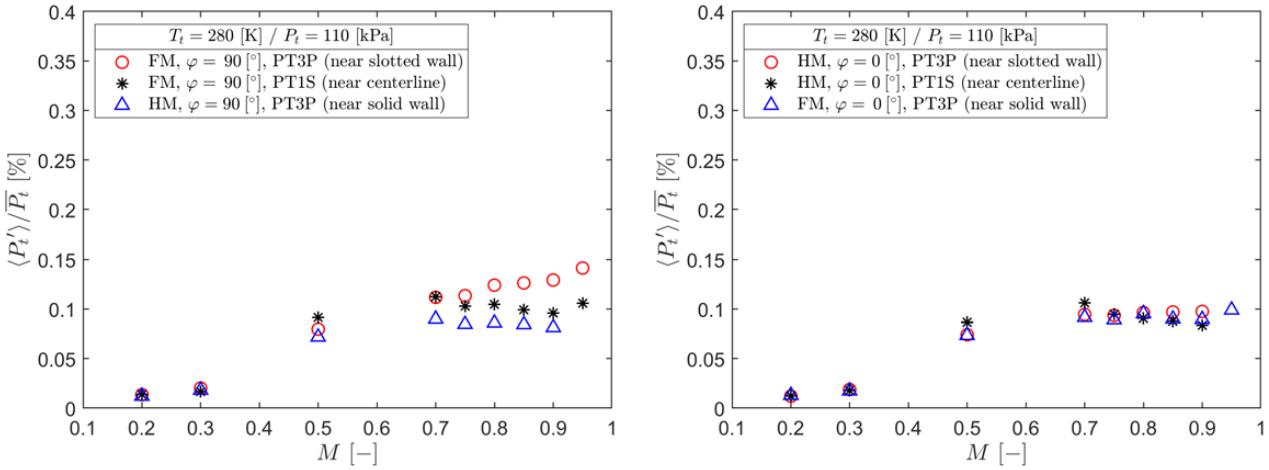


(a) FM wall configuration, $\varphi = 90°$

(b) HM wall configuration, $\varphi = 0°$

Figure 29 – Comparison of total pressure fluctuations between slotted and solid walls.

**Spectral characteristics** In Fig. 30, spectral characteristics of total pressure fluctuations near the tunnel centerline are compared for two Reynolds number groups at Mach 0.5. This Mach number has been selected as at this Mach number the most remarkable Reynolds effect was observed in Fig. 27(a). In order to eliminate temperature effects, a dimensionless frequency $f_c$, made by use of tunnel static temperature, is introduced (see Fig. 30(b)). The comparative analysis indicates that the amplitude and frequency characteristics of the total pressure fluctuation close to the test section centerline depends on both the Reynolds number and the static temperature. The Reynolds number effect is however limited for low frequencies. Significant amplitudes observed at high frequencies are due to acoustic disturbances (Helmholtz resonance) caused by some circular cavities of small diameter (ca. 3 mm) presented in the test section walls. The levels decrease remarkably, if the cavities are not present (verified during the second FQA entry).

Spectral characteristics for the FM slots are compared with those of solid walls at Mach 0.85 and given in Fig. 31(a). As expected, the spectral characteristics obtained from the outboard probe near the solid top wall is similar to those near the test section centerline. Comparing these with the spectral characteristics for the FM slots, the frequency range, which is affected by the slot influence, is easy to detect. A similar finding is also made for the HM walls (see Fig. 31(b)).

The Reynolds number dependency of the slot flow caused characteristics is shown in Fig. 32(a) for both the low and high Reynolds number test-points. This becomes even better visible when comparing for each Reynolds number the spectral characteristics for the slotted top wall (FM wall configuration) measured by the outboard probe PT3P with those for the inboard probe PT1S measuring total pressure fluctuation near the test section centerline (see Fig. 32(b)).

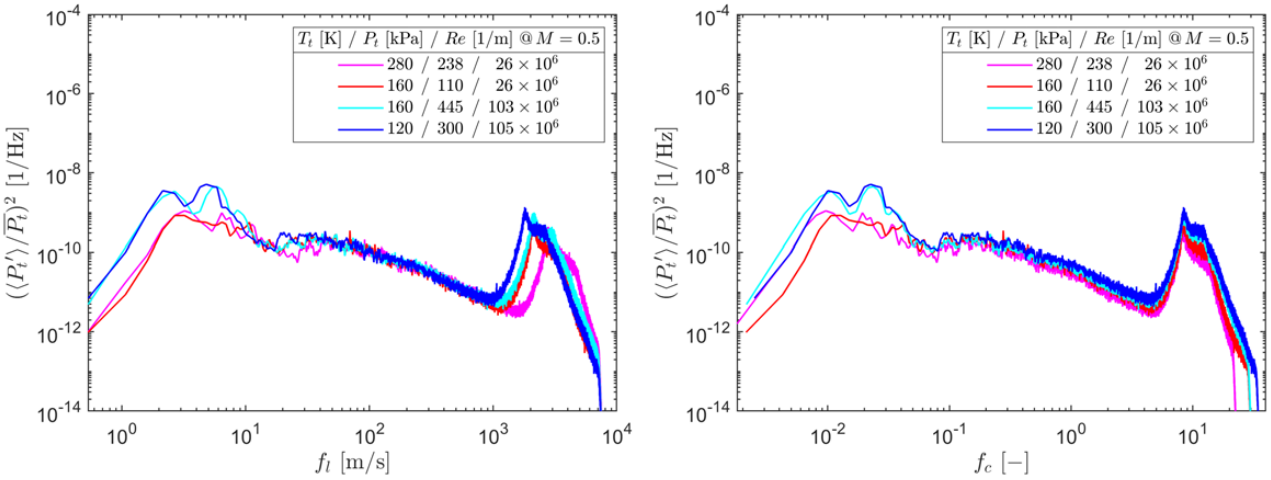


(a) Non-dimensionless frequency

(b) Dimensionless frequency

Figure 30 – Reynolds number and static temperature dependency of total pressure fluctuation near the test section centerline (PT1S, FM wall configuration, $\varphi = 0°$ and $M = 0.5$).

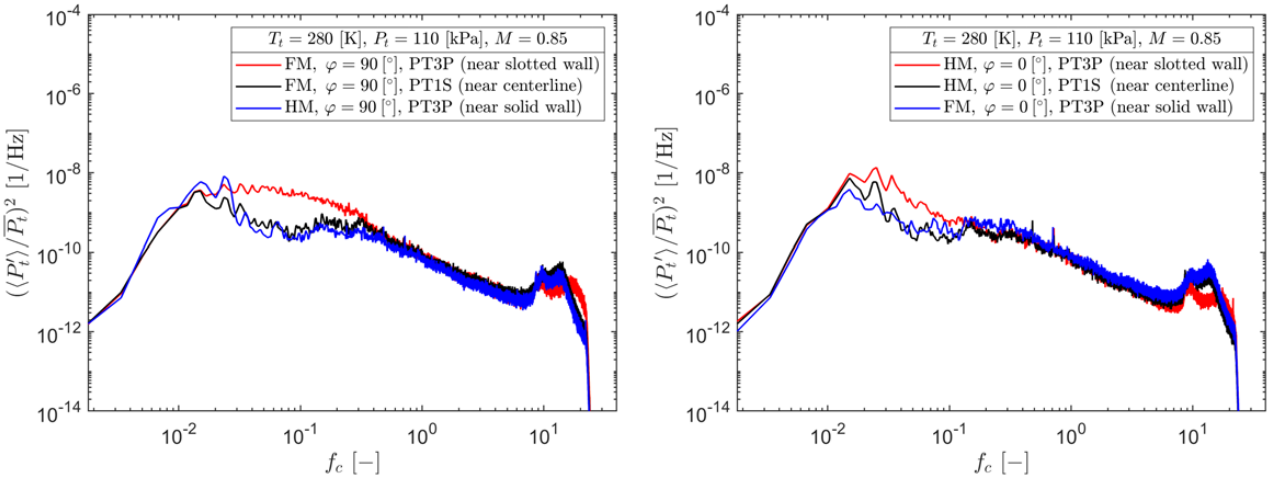


(a) FM wall configuration, $\varphi = 90°$

(b) HM wall configuration, $\varphi = 0°$

Figure 31 – Comparison of spectral characteristics between slotted and solid walls at $M = 0.85$.

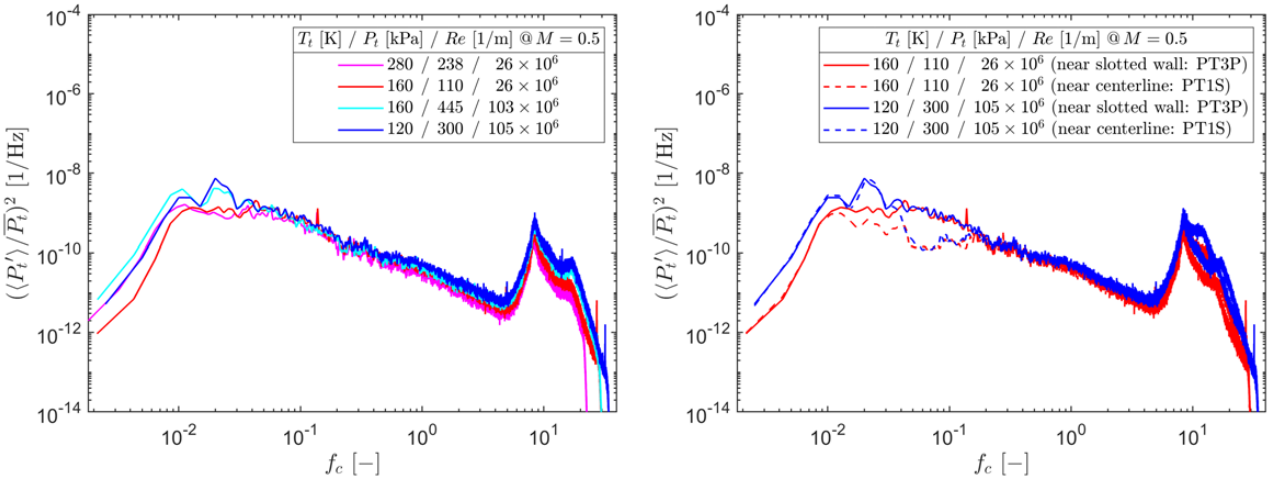


(a) Outboard probe: PT3P

(b) Outboard & inboard probe: PT3P & PT1S

Figure 32 – Reynolds number dependency of total pressure fluctuation near the slotted top wall (FM wall configuration, $\varphi = 90°$ and $M = 0.5$).

### 5.1.2 Velocity Fluctuations

**Velocity fluctuation spatial homogeneity** Fig. 33 presents lateral and angular distributions of fluctuating axial and lateral flow velocity for the FM wall configuration and for two Mach numbers ($M = 0.3$ and $M = 0.75$). At the low Mach number, similar to the total pressure fluctuations at high Mach number, the outboard hot-wire probes (HW1 and HW3) measure higher flow velocity fluctuations, if they are located near the slotted top (HW1) and bottom wall (HW6). At the high Mach number ($M = 0.75$), the situation is different: the fluctuation of axial component measured by the outboard hot-wire probes near the slotted walls is no longer significant, while the pronounced fluctuation of the lateral component is still visible at this Mach number (see Fig. 33(b) and Fig. 33(d)). At high Mach numbers, the axial component of flow filed in the region of the slotted walls might be superimposed on the high-speed mean flow, while keeping the lateral component its characteristics. The results of the inboard hot-wire probe measurements (HW2, HW3, HW4 and HW5) show homogeneous lateral as well as angular distributions of test section flow field and do not indicate any significant influences of both slotted and solid walls for both axial and lateral velocity components. Note that not all hot-wire probe results are presented in the figures as some probes failed during the test. A similar finding can also be made for the HM wall configuration (see Fig. 34). Similar to the observation of the total pressure probes, the fluctuation levels, measured by the outboard probe, are lower than those for the FM wall configuration due to the larger distance between the probes and the slotted walls. In any case, the slotted wall influence significantly decreases with increasing distance from the walls in a consistent manner.

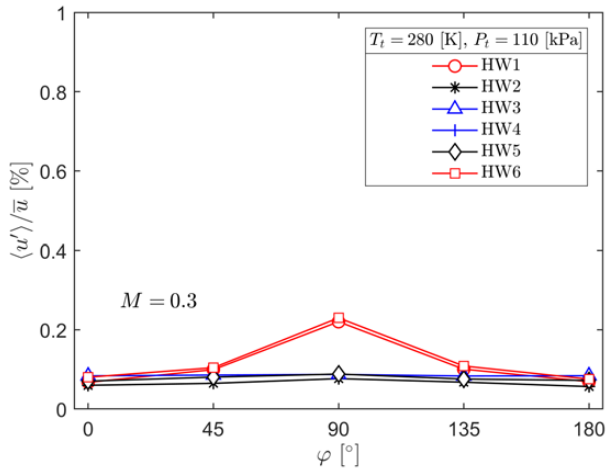


(a) Axial component @ $M = 0.3$

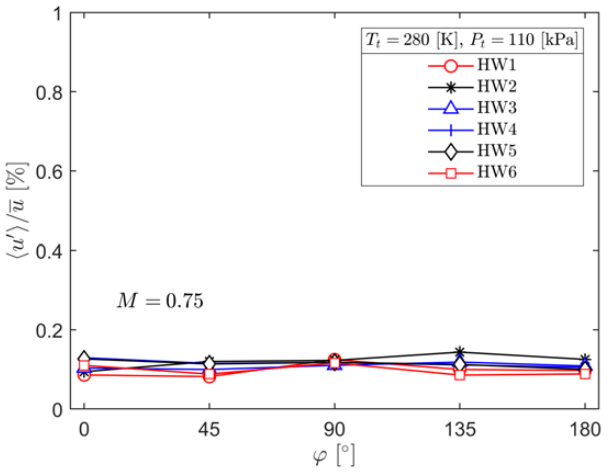


(b) Axial component @ $M = 0.75$

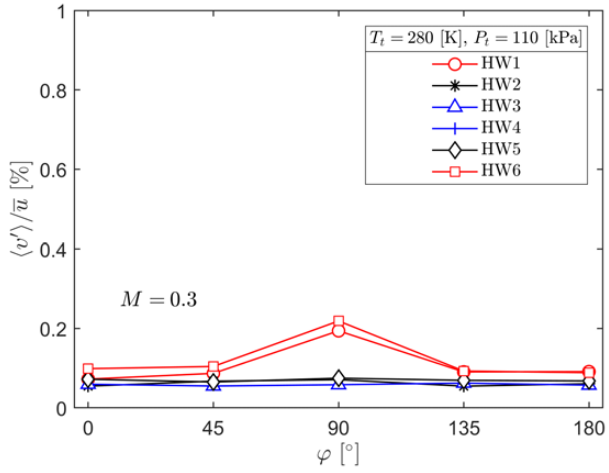


(c) Lateral component @ $M = 0.3$

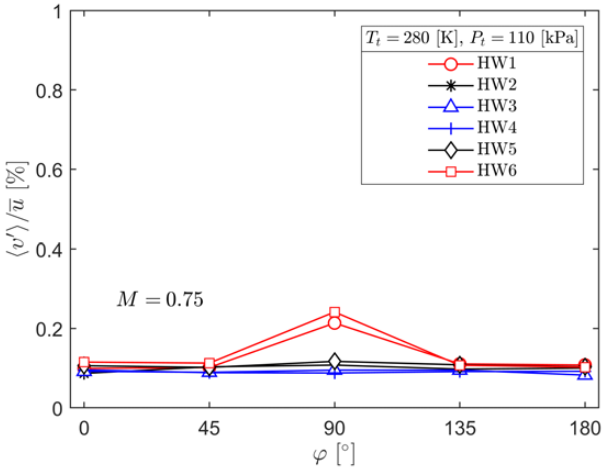


(d) Lateral component @ $M = 0.75$

Figure 33 – Lateral and angular distributions of fluctuating velocity (FM slotted walls).

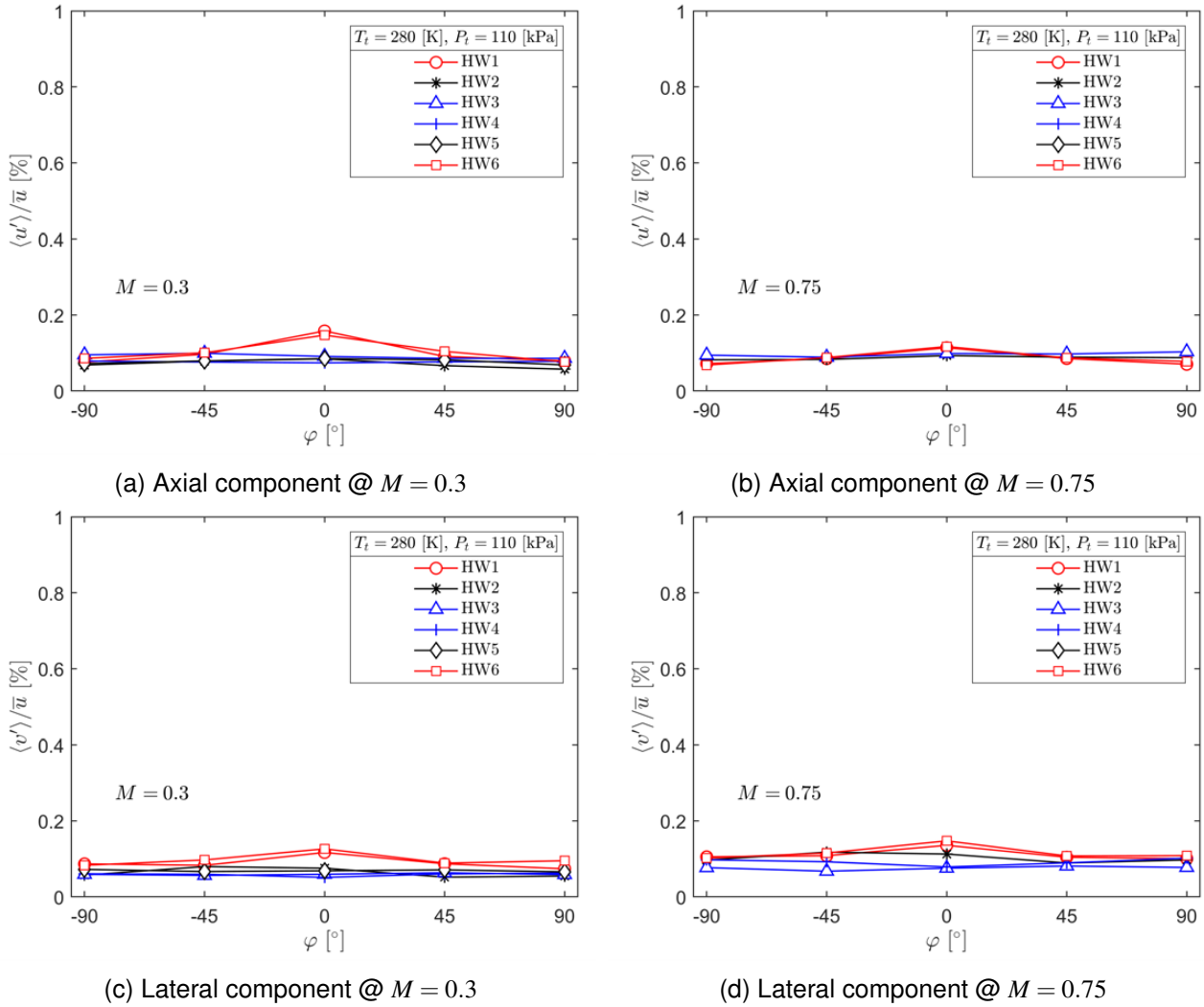


(a) Axial component @ $M = 0.3$

(b) Axial component @ $M = 0.75$

(c) Lateral component @ $M = 0.3$

(d) Lateral component @ $M = 0.75$

Figure 34 – Lateral and angular distributions of fluctuating velocity (HM slotted walls).

**Influence of Mach number** In Fig. 35 and Fig. 36, fluctuations of axial and lateral component of the flow field near the slotted bottom wall ($\varphi = 90°$, HW6) and of the flow field near the test section centerline ($\varphi = 0°$, HW3) are presented as a function of test-section Mach number for the FM slotted wall configuration. The axial component of the flow field near the slotted wall tends to lower fluctuations with increasing flow speed. The effect of Reynolds number on the axial component fluctuations also seems to be becoming small at the high Mach numbers. Near the tunnel centerline, the Mach number dependency of fluctuating velocity components is less significant than the Reynolds effect. It is interesting that only the outboard hot-wire probe (HW6), measuring near the slotted bottom wall, show a pronounced influence of Mach number control method (trim flap control) on the velocity fluctuation (see Fig. 35(a) and Fig. 36(a)).

**Solid wall influences** The Mach number dependency of the flow field near the slotted wall is compared with that for the solid wall, as given in Fig. 37. Similar to the analysis for the total pressure probe, both the level and characteristics of axial and lateral velocity fluctuations near the solid wall is comparable with those near the tunnel centerline, indicating that, in contrast to the slotted wall, the solid walls do not lead to any significant flow unsteadiness near the wall flow field.

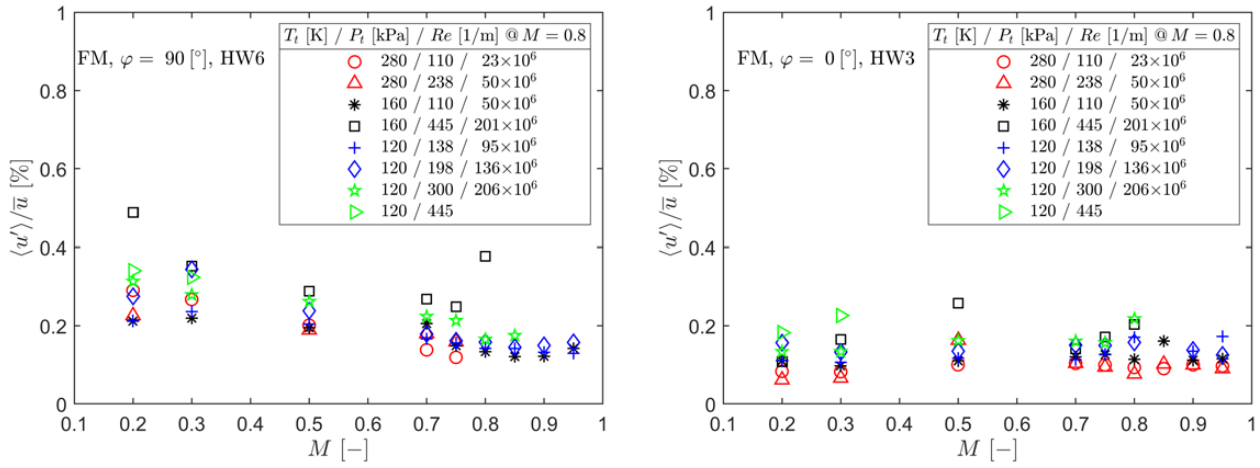


(a) Near the slotted bottom wall ($\varphi = 90°$, HW6) (b) Near the test-section centerline ($\varphi = 0°$, HW3)

Figure 35 – Axial velocity fluctuations (FM slotted wall configuration).

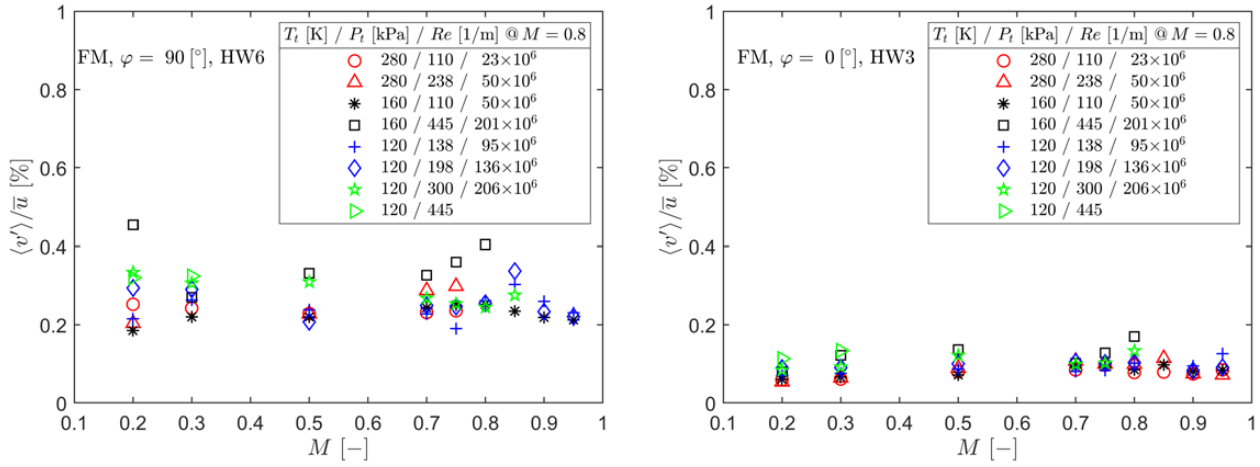


(a) Near the slotted bottom wall ($\varphi = 90°$, HW6) (b) Near the test-section centerline ($\varphi = 0°$, HW3)

Figure 36 – Lateral velocity fluctuations (FM slotted wall configuration).

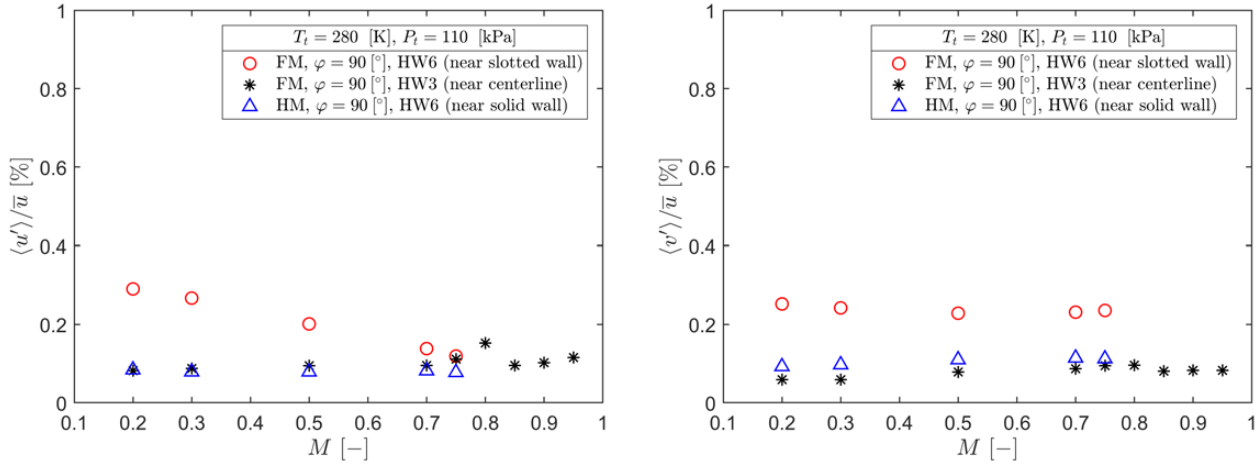


(a) Axial components (b) Lateral components

Figure 37 – Comparison of velocity fluctuations between the slotted and solid bottom wall.

**Spectral characteristics** Spectral characteristics of the flow field near the slotted top wall ($\varphi = 90°$, HW1) for the FM wall configuration and near the slotted sidewall for the HM test case ($\varphi = 0°$, HW1) are analyzed in Fig. 38 and Fig. 39, respectively. The spectral characteristics of the fluctuating axial component for both the FM and HM wall configuration are quite similar to those observed by the evaluation of total pressure probes (see Fig. 31(a) and Fig. 31(b)). The affected frequency range is also comparable to the findings from the analysis of the total pressure fluctuations. Spectral characteristics of the lateral component are slightly different to those of axial component irrespective of whether they are subject to the slot influence or not.

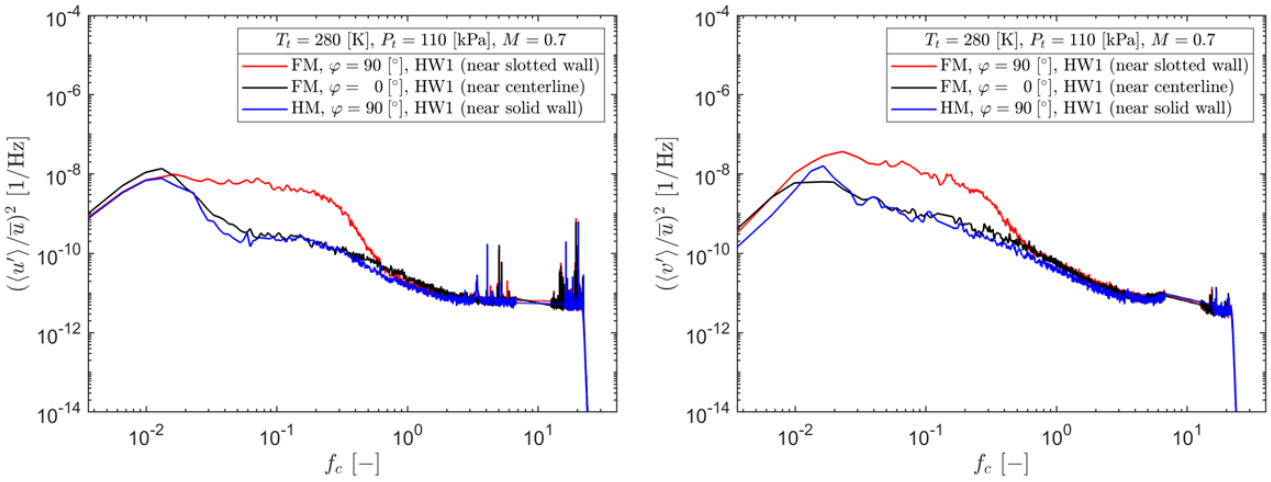


(a) Axial components (b) Lateral components

Figure 38 – Comparison of spectral characteristics of velocity fluctuations between the slotted and solid bottom wall ($M = 0.7$).

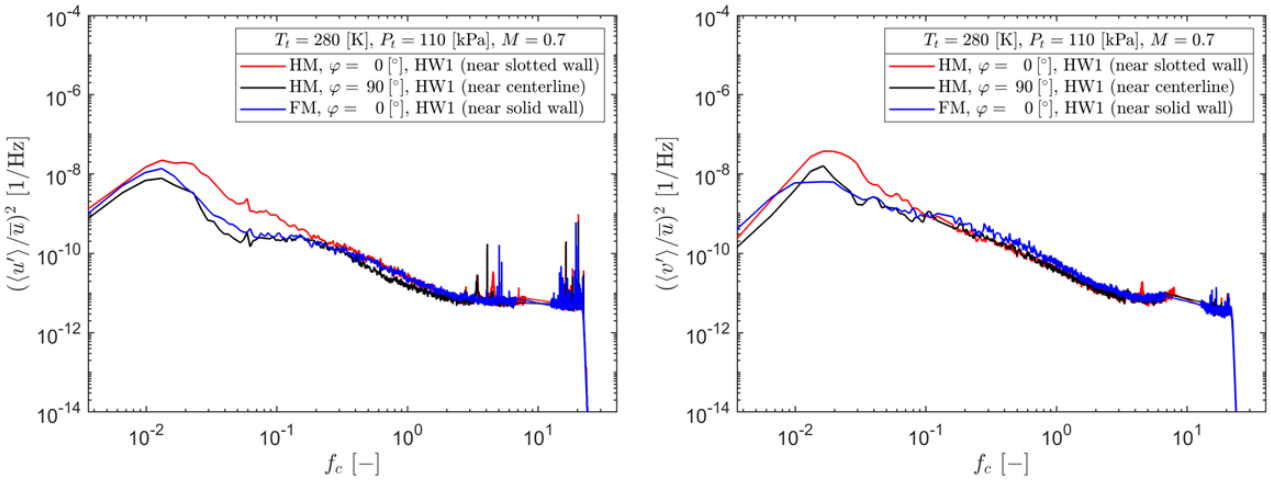


(a) Axial components (b) Lateral components

Figure 39 – Comparison of spectral characteristics of velocity fluctuations between the slotted and solid sidewall ($M = 0.7$).

Based on the analysis of both the pressure and velocity fields, it is concluded that the flow characteristics in ETW's test volume is sufficiently homogeneous for both wall configurations. The slot influences in terms of pressure and velocity fluctuations are identified for both wall configurations. However, they are locally limited and have no measurable impact on the inflow near the model position in both, the FM and HM model test set-up configuration.

## 5.2 Mach Number Control Methods

Fig. 40 reveals Mach number deviations made by subtraction of test-section Mach numbers, measured by the standard FRS close to the test section entry, from the nominal Mach numbers ($M = 0.75$, $0.85$ and $0.95$) for three different Mach number control methods. The data were obtained during the second FQA entry at the test condition $T_t = 280$ K and $P_t = 110$ kPa. In general, the standard second throat control method reveals the most stable Mach number control over time at all Mach numbers considered. At Mach 0.75, the trip-flap control mode shows a rather unstable Mach number controlling. The Mach number fluctuations however become more stable with increasing Mach number and at the highest Mach number tested ($M = 0.95$), the trip flap control also achieves a control quality as good as the standard combined method.

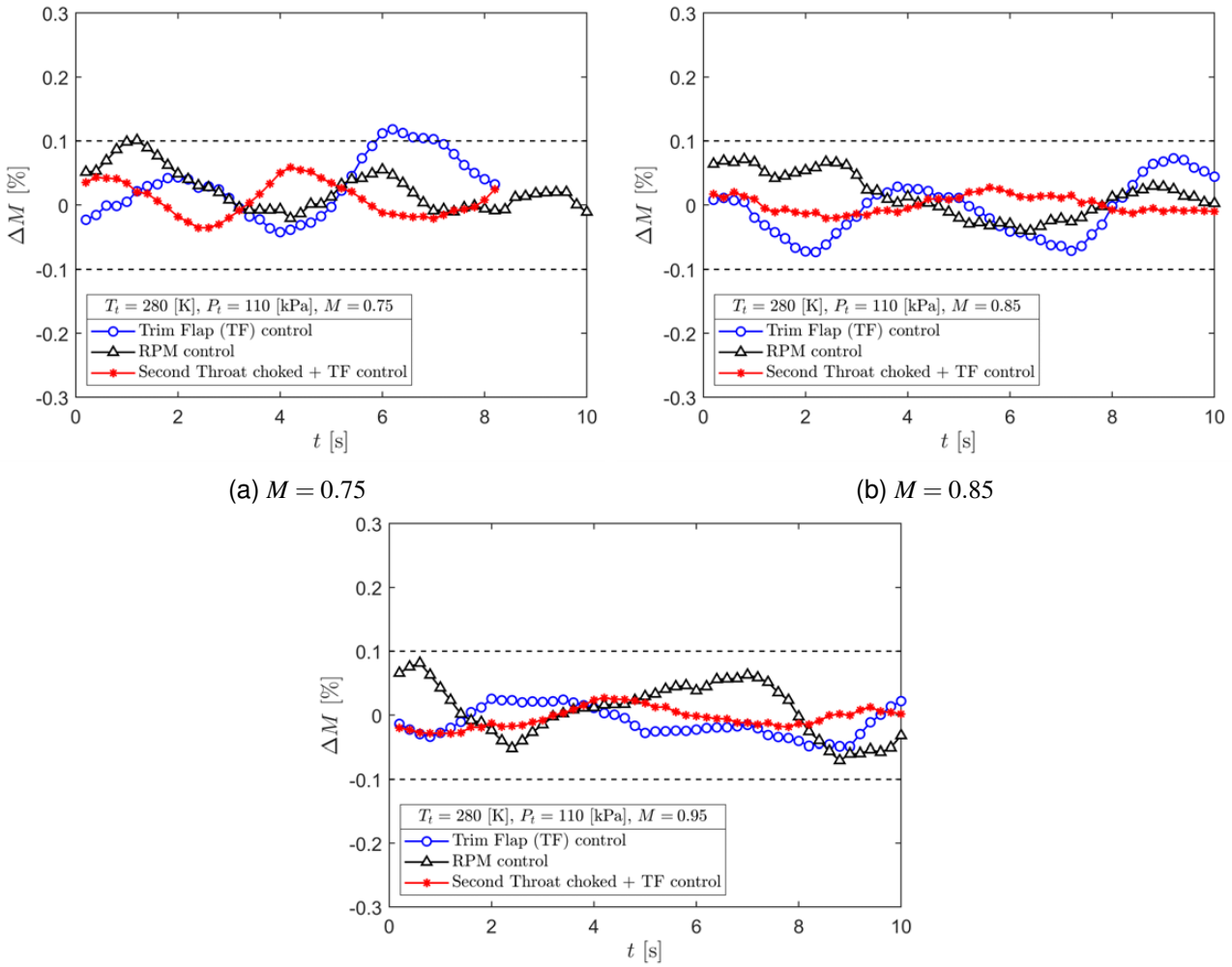


(a) $M = 0.75$ (b) $M = 0.85$

(c) $M = 0.95$

Figure 40 – Comparison of ETW's different Mach number control methods.

Fig. 41(a) and Fig. 41(b) present static pressure fluctuations, measured by the flush-mounted unsteady static pressure transducers (Kulite) upstream (TS-up) and downstream (TS-down) of the model reference position (see also Fig. 41(d)). In addition, static pressure fluctuations in the entry region of the high-speed diffuser (HSD-top) are shown in Fig. 41(c). As expected, the tunnel static pressure field experiences the lowest fluctuations when the second throat is choked and the trim flap directly controls the Mach number. The static pressure field tends to have less fluctuations with increasing flow speed. Significant levels of fluctuating static pressure are observed at Mach 0.75 and for the control mode using the trim flap unchocked. Furthermore, at the high Mach numbers ($M = 0.80$ and $M = 0.95$), both the RPM and trim flap unchoked control modes show significantly lower fluctuations, almost the same as that to the choked method. In contrast to the test section, the choked method leads to the highest static pressure fluctuations in the high-speed diffuser because of com-

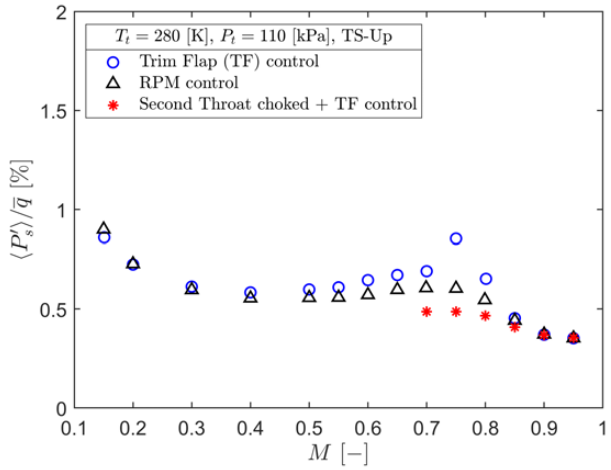


(a) Test section upstream (TS-up)

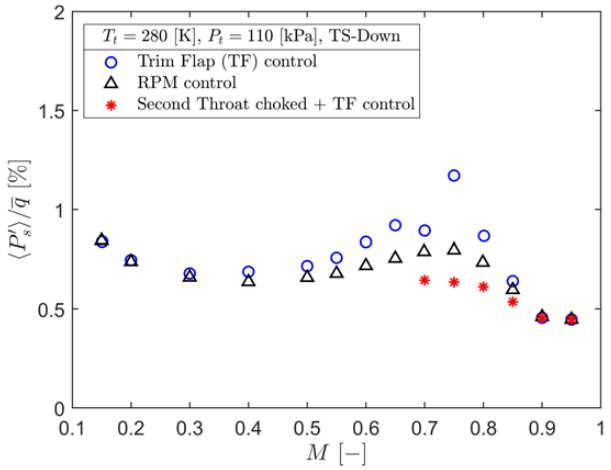


(b) Test section downstream (TS-down)

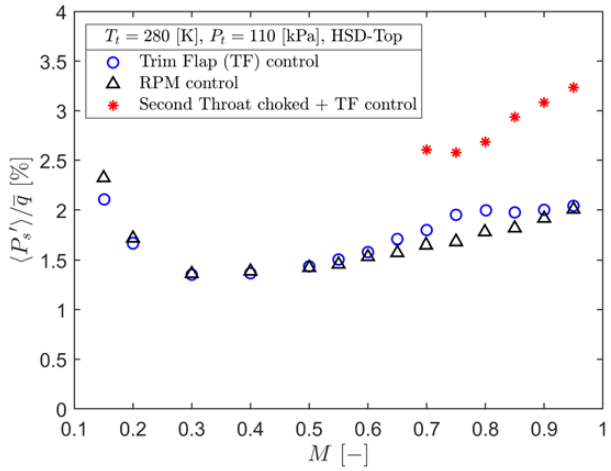


(c) High-speed diffuser (HSD-top)

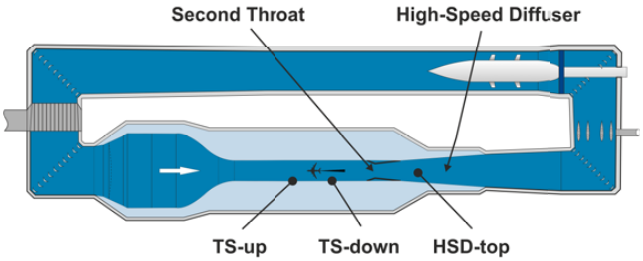


(d) Location of flush-mounted static pressure probes.

Figure 41 – Static pressure fluctuation at different Mach number control methods.

pression shocks downstream of the second throat, which in turn causes an instantaneous increase of the static pressure and thus the higher fluctuations.

In Fig. 42, spectral characteristics of the static pressure fluctuations are analysed at three Mach numbers. At $M = 0.75$, significant peaks are identified for the trim flap unchoked mode. It explains the remarkably high fluctuation levels, observed in Fig. 41(a) and Fig. 41(b). The observed frequencies correspond to the test section width as well as the height. Therefore, it is suspected that there might be an interaction between the re-entry flow and the blocking effect of the trim flaps. The combined method, which is the ETW's standard Mach number control procedure at this Mach number and uses also the trim flap choked control, do not induce these peaks, possibly because the flap deployment angle for the combined mode is much lower than that for the trim flap only mode. At Mach 0.85, these peaks are significantly decreased, and at $M = 0.95$ they have completely disappeared. At this Mach number, the spectral characteristics of all three Mach control methods are very similar to each other, explaining also the similar fluctuation levels between the Mach number control modes, observed in Fig. 41(a) and Fig. 41(b).

Fig. 43 presents the total pressure fluctuation obtained during the first FQA entry for two test points of similar Reynolds number, but used different Mach number control methods at $M = 0.75$ and at $M = 0.90$. As the frequency of these peaks scales with speed of sound, the observation likely relates to an acoustic resonance phenomenon. The analysis also indicates that the phenomenon mainly depends on the Mach number control method and the test-section Mach number rather than the Reynolds number.

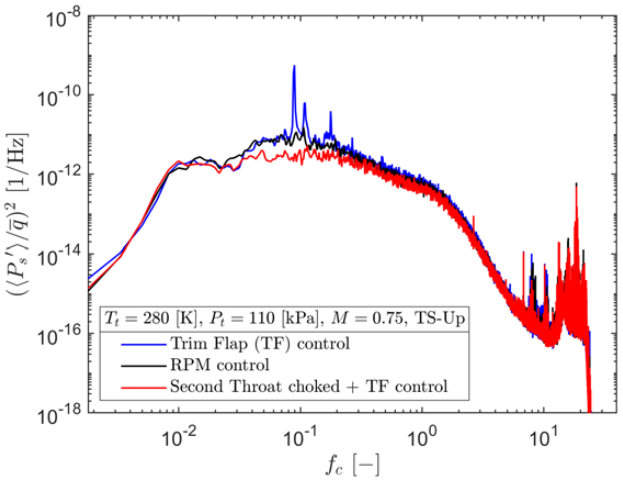


(a) $M = 0.75$

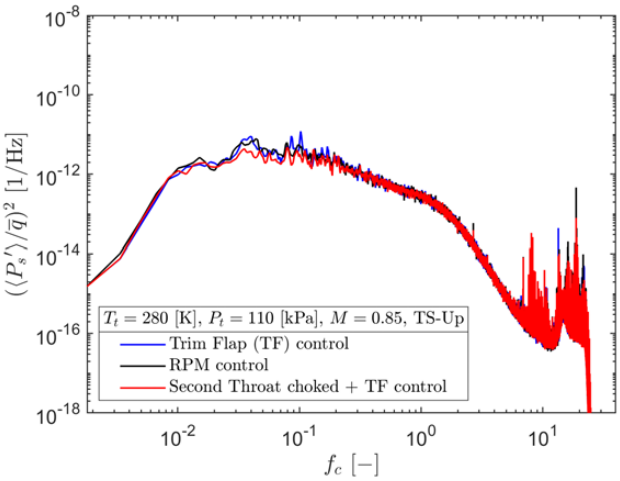


(b) $M = 0.85$

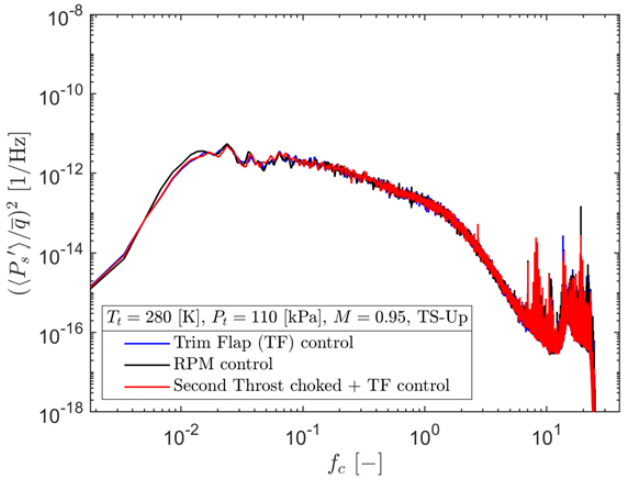


(c) $M = 0.95$

Figure 42 – Spectral characteristics of static pressure fluctuation for three different Mach number control methods.

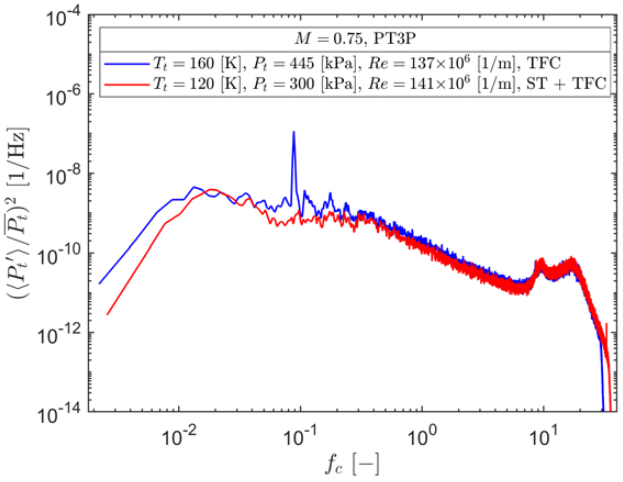


(a) $M = 0.75$

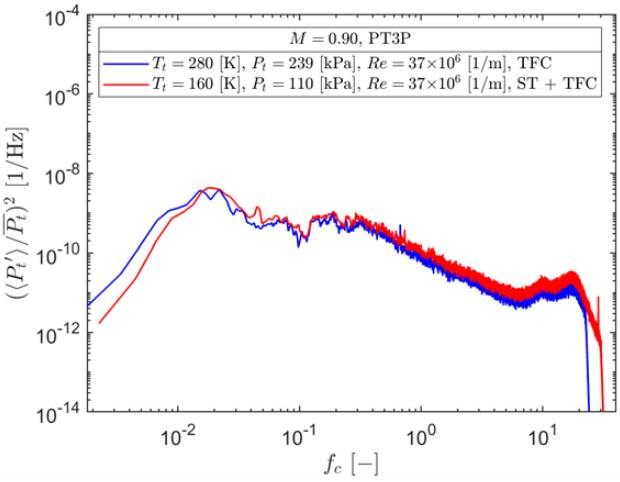


(b) $M = 0.90$

Figure 43 – Comparison of trim flap unchoked method (TFC) and combined method (ST + TFC) in terms of spectral characteristics of total pressure fluctuation obtained from the first FQA entry (FM wall configuration, $\varphi = 0^\circ$ and outboard probe PT3P).

## 6. Conclusion and Outlook

The paper summarises ETW's recent unsteady flow quality assessment, including a description of the employed test setup and its calibration. For typical test section configurations, over a wide range of ETW's operating Mach and Reynolds numbers, a comprehensive unsteady flow-quality reference dataset for the empty test section has been acquired.

The resulting dataset includes spectral characteristics of the flow cleaned from sensor setup related artifacts and focus on a frequency range from 10 Hz to 30,000 Hz as it is considered relevant for test related to transitional boundary layer receptivity, buffet or aeroelastic phenomena. The results of the first test entry indicated that the unsteady flow characteristics is sufficiently homogeneous across ETW's test volume with respect to both the velocity and pressure fluctuations. The analysis revealed some very localised impacts on the characteristics close to the wall slots, which shows no measurable impact on the inflow near the model position in both, the FM and HM model test set-up configurations. In addition, the solid walls do not show any significant influences on the test-section flow characteristics in terms of the velocity and pressure field fluctuations.

The second test entry has improved the understanding of how ETW's Mach number control methods affect the test-section unsteady flow characteristics. It confirmed that the second throat combined with the trim flap choked control, which is ETW's standard method at the high speeds ($M > 0.7$), enables maintaining the test-section Mach number stable ($\Delta M < 0.1\,\%$) and also ensures the lowest pressure fluctuations in the test volume. Higher pressure disturbances were observed when using the trim flap only unchoked method at certain Mach numbers. This will be further investigated in order to enhance its unsteady flow quality because this Mach number control method is otherwise attractive as it allows less energy consuming tunnel operation.

## Contact Author Email Address

mailto: jhy@etw.de

## Acknowledgments

The authors thank the German Federal Ministry for Economic Affairs and Climate Action LuFoV-3 project LoCaRe (2018-2021), which enabled this work under grant agreement no 20A1701A by funding. The support of the hot-wire measurements and data analysis by Dr. R. Meyer from the department of engine acoustics of the Institute of Propulsion Technology at the German Aerospace Centre (DLR) based on his esteemed expertise is gratefully acknowledged. Sincere thanks to J. Quest for his dedicated support of these investigations and valuable discussions. The authors would like to thank apl. Prof. Dr. C. Breitsamter from the Chair of Aerodynamics and Fluid Mechanics at the Technical University of Munich for providing the hot-wire calibration facility. The authors also wish to thank all ETW colleagues for their permanent assistance during the test campaigns.

## References

[1] Quest J. ETW – Flow Quality Aspects and First Model Tests. *20th Congress of the International Council of Aeronautical Sciences*, Sorrento, Italy, ICAS-96-1.5.1, pp 1023-1032, 1996.

[2] Quest J. ETW – High Quality Test Performance in Cryogenic Environment. *21st AIAA Aerodynamic Measurement Technology and Ground Testing Conference*, Denver, Colorado, AIAA 2000-2206, 2000.

[3] Streit T et al. Complementary Numerical and Experimental Data Analysis of the ETW Telefona Pathfinder Wing Transition Tests. *49th AIAA Aerospace Sciences Meeting including the New Horizons Forum and Aerospace Exposition*, Orlando, Florida, AIAA 2011-881, 2011.

[4] Wright M. Development of the Half Model Testing Capability at ETW. *22nd Congress of the International Council of Aeronautical Sciences*, Harrogate, UK, ICA0374, 2000.

[5] Fey U et al. Transition Detection by Temperature Sensitive Paint at Cryogenic Temperatures in the European Transonic Wind Tunnel. *20th International Congress on Instrumentation in Aerospace Simulation Facilities*, Göttingen, Germany, pp 77-88, 2003.

[6] ETW GmbH. *ETW User Guide*. Revision A, ETW/D/95001/A, 2004.

[7] Green J and Quest J. A Short History of the European Transonic Wind Tunnel ETW. *Progress in Aerospace Sciences*. Vol. 47, No. 5 pp 319-368, 2011.

[8] Quix H and Quest J. Hot-Wire Measurements in Cryogenic Environment. *49th AIAA Aerospace Sciences Meeting including the New Horizons Forum and Aerospace Exposition*, Orlando, Florida, AIAA 2011-880, 2011.

[9] Quix H, Quest J and Brzek C. Hotwires in pressurized, cryogenic environment – It works!. *50th AIAA Aerospace Sciences Meeting including the New Horizons Forum and Aerospace Exposition*, Nashville, Tennessee, AIAA 2012-0105, 2012.

[10] Dantec Dynamics. *Probe for Hot-wire Anemometry*. Publication No.: 238v11.

## Copyright Statement